Chemosphere 350 (2024) 141049

Contents lists available at ScienceDirect

Chemosphere

journal homepage: www.elsevier.com/locate/chemosphere

Predominance of the alkaline earth(II) triscarbonatoactinyl(VI) complexes in different geochemical contexts: Review of existing data and estimation of potentially unidentified species

Pascal E. Reiller

Université Paris-Saclay, CEA, Service de Physico-Chimie (SPC), F-91191, Gif-sur-Yvette CEDEX, France

HIGHLIGHTS

- The thermodynamic data of alkaline earth (II)carbonatouranylate (VI) are reviewed.
- Linear free energy relationships are proposed to estimate Pu(VI) and Np(VI) complexes.
- Complexation constants are tested in different geochemical contexts.
- Predominance of the alkaline earth (II) carbonatoactinylate (VI) complexes are estimated.

GRAPHICAL ABSTRACT

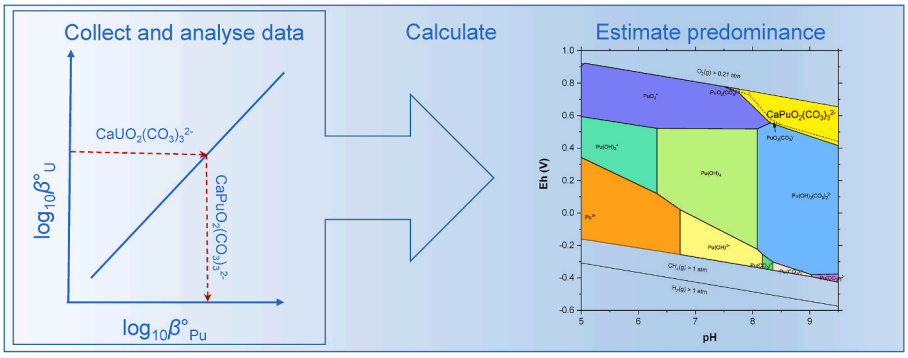

ARTICLE INFO

Handling Editor: Milena Horvat

Keywords:
Uranium
Actinides
Carbonate complexes
Alkaline earth metals

ABSTRACT

From the available thermodynamic data in the literature, a review of the impact of the formation of complexes between triscarbonatoactinyl(VI) and alkaline earth(II) (Ae) is estimated under varying conditions. First, after analyzing the literature data and using the ascertained thermodynamic data available from the commissioned reviews from the Nuclear Energy Agency (Organization for the Economic Cooperation and Development) Thermochemical DataBank Project on actinides (An) U, Np, and Pu, and from recently determined $Ae_nUO_2(CO_3)_3^{(4-2n)-}$ thermodynamic functions, the formation of $Ae_nAnO_2(CO_3)_3^{(4-2n)-}$ complexes for Pu(VI) and Np(VI) are estimated using linear free energy relationships (LFERs). The data are in good agreement with the sole determination of $AePuO_2(CO_3)_3^{2-}$ from Jo et al. (Dalton Trans. 49, 11605), which gives a relative confidence in the LFERs, and allows the application to actual situations. From existing uranium data, first, the impact of the origin of the data on the calculated predominance is addressed under 0.1 M NaCl and atmospheric CO_2(g); second, the influence of ionic strength and salinity on predominance is estimated; and finally, the influence of temperature up to 50 °C on the solubility of uraninite in a deep geological radioactive waste storage or disposal site is calculated. For neptunium and plutonium, the impact of the potential $\log_{10}\beta^\circ(Ae_nAnO_2(CO_3)_3^{(4-2n)-})$ on Pourbaix diagrams of Pu and Np in Mg–Ca–CO_3 media are estimated from Jo et al. (Dalton Trans. 49, 11605) and LFERs. Finally, the application to the speciation of Pu and Np in seawater is proposed.

E-mail address: pascal.reiller@cea.fr.

https://doi.org/10.1016/j.chemosphere.2023.141049
Received 12 October 2023; Received in revised form 1 December 2023; Accepted 26 December 2023
Available online 3 January 2024
0045-6535/© 2024 Elsevier Ltd. All rights reserved.

1. Introduction

The complexes between triscarbonatouranyl(VI) and alkaline earth (II) — afterwards noted Ae(II) — have been the subject of several studies since their discovery in uranium mine seepage waters (Bernhard et al., 1996). The general stoichiometry $Ae_nUO_2(CO_3)_3^{(4-2n)-}$ (n = {1, 2}) have been evidenced throughout the alkaline earth series from Mg to Ba (Bernhard et al., 1996, 1998, 2001; Dong and Brooks, 2006, 2008; Endrizzi et al., 2016; Geipel et al., 2008; Jo et al., 2019a, 2019b; Kalmykov and Choppin, 2000; Lee et al., 2017; Lee and Yun, 2013; Maia et al., 2021; Shang and Reiller, 2020, 2021a, 2021b; Shang et al., 2020). These complexes represent the vast majority of the species in uranium-containing carbonated waters (Gardner et al., 2022; Lartigue et al., 2020; Reiller and Descostes, 2020; Shang et al., 2023) even in reducing conditions such as envisaged underground radioactive waste storage sites (Grivé et al., 2015; Montavon et al., 2022; Montoya et al., 2021; Reiller and Descostes, 2020; Tullborg et al., 2017).

Up to very recently (Grenthe et al., 2020), no thermochemical functions or constants of formation for these species were selected by the widely recognized commissioned selection for the Thermochemical Data Base (TDB) project of the Nuclear Energy Agency-Organization for Economic Cooperation and Development (NEA-OECD https://www.oecd-nea.org/jcms/pl_22166/thermochemical-database-tdb-project) in Guillaumont et al. (2003). Despite the interest that these species have aroused, the data that allowed an extrapolation to infinite dilution, necessary to estimate the thermochemical functions of formation, were relatively scarce (Dong and Brooks, 2008; Kalmykov and Choppin, 2000; Shang and Reiller, 2020, 2021a; Shang et al., 2020). Moreover, in the first years, only $Ca_2UO_2(CO_3)_3$(aq) was evidenced (Bernhard et al., 1996; Kalmykov and Choppin, 2000); $CaUO_2(CO_3)_3^{2-}$ was first suggested by Bernhard et al. (2001). This prevented the selection of specific ion-interaction theory (SIT) coefficient ε for these species in Grenthe et al. (2020). Shang et al. (Shang and Reiller, 2020, 2021a; Shang et al., 2020) — who published their results after the cut-off date of the latter NEA-OECD review (Grenthe et al., 2020) —, proposed $\log_{10}\beta^\circ$ and ε values for the $Ae_nUO_2(CO_3)_3^{(4-2n)-}$ species in NaCl and $NaClO_4$. They also shown a good agreement between all values in the literature.

The environmental importance of these species has been recognized in various fields of research (Carvajal et al., 2012; Crançon et al., 2012; Doughman et al., 2024; Liu et al., 2007; Xie et al., 2021). They have been evidenced spectroscopically in situ (Bernhard et al., 1996; Maloubier et al., 2015; Prat et al., 2009; Shang et al., 2023; Tullborg et al., 2017). The structure of the $Ae_nUO_2(CO_3)_3^{(4-2n)-}$ complexes was ascertained in EXAFS (Bernhard et al., 2001; Brooks et al., 2003; Kelly et al., 2005, 2007), and calculated in molecular dynamics and ab initio (Oher et al., 2020; Priest et al., 2016; Tirler and Hofer, 2016).

Knowing the similarities between the chemistry of the actinides (An) at their + VI redox state (Vercouter, 2021; Vitorge, 1999; Vitorge and Capdevila, 2003), the question of the formation of eventual $Ae_nAnO_2(CO_3)_3^{(4-2n)-}$ species for Np(VI) and Pu(VI) was pending. Very recently, Jo et al. (2020) evidenced the formation of $MgPuO_2(CO_3)_3^{2-}$ and $CaPuO_2(CO_3)_3^{2-}$ in visible-near-infrared absorption spectroscopy at 0.1 M H/$NaClO_4$ ionic strength. These experiments allowed the authors to propose thermodynamic constants extrapolated to infinite dilution using the Davies (1962) equation. The general conditions under which these species can be dominant in geochemical media are somewhat

Table 1
Selected thermodynamic constants $\log_{10}\beta^\circ$(An) of common inorganic species of An = {U; Np; Pu}.

Equilibrium	$\log_{10}\beta^\circ$(U)	$\log_{10}\beta^\circ$(Np)	$\log_{10}\beta^\circ$(Pu)
$An^{4+} + H_2O \rightleftarrows An(OH)^{3+} + H^+$	−0.54 ± 0.06[a]	0.55 ± 0.20[d]	0.60 ± 0.20[b]
$An^{4+} + 2H_2O \rightleftarrows An(OH)_2^{2+} + 2H^+$	−1.90 ± 0.20[e]	0.35 ± 0.30[d]	0.60 ± 0.30[b]
$An^{4+} + 3H_2O \rightleftarrows An(OH)_3^+ + 3H^+$	−5.20 ± 0.40[e]	–	−2.30 ± 0.40[b]
$An^{4+} + 4H_2O \rightleftarrows An(OH)_4(aq) + 4H^+$	−10.01 ± 1.40[d]	−8.31 ± 1.10[d]	−8.50 ± 0.50[b]
$AnO_2^+ + H_2O \rightleftarrows AnO_2(OH)(aq) + H^+$	–	−11.30 ± 0.70[d]	−11.50 ± 0.12[c]
$AnO_2^{2+} + H_2O \rightleftarrows AnO_2(OH)^+ + H^+$	−5.25 ± 0.24[e]	−5.10 ± 0.40[d]	−5.50 ± 0.50[d]
$AnO_2^{2+} + 2H_2O \rightleftarrows AnO_2(OH)_2(aq) + 2H^+$	−12.15 ± 0.07[d]	–	−13.20 ± 1.50[b]
$2AnO_2^{2+} + 2H_2O \rightleftarrows (AnO_2)_2(OH)_2^{2+} + 2H^+$	−5.62 ± 0.08[e]	−6.27 ± 0.21[d]	−7.50 ± 1.00[b]
$3AnO_2^{2+} + 5H_2O \rightleftarrows (AnO_2)_3(OH)_5^+ + 5H^+$	−15.55 ± 0.12[e]	−17.12 ± 0.22[d]	–
$An^{4+} + F^- \rightleftarrows AnF^{3+}$	9.42 ± 0.51[d]	8.96 ± 0.14[d]	8.84 ± 0.10[b]
$An^{4+} + 2F^- \rightleftarrows AnF_2^{2+}$	16.56 ± 0.71[d]	15.70 ± 0.30[d]	15.70 ± 0.20[b]
$AnO_2^{2+} + F^- \rightleftarrows AnO_2F^+$	5.16 ± 0.06[e]	4.57 ± 0.07[d]	4.56 ± 0.20[b]
$AnO_2^{2+} + 2F^- \rightleftarrows AnO_2F_2(aq)$	8.83 ± 0.08[e]	7.60 ± 0.08[d]	7.25 ± 0.45[b]
$An^{4+} + Cl^- \rightleftarrows AnCl^{3+}$	1.72 ± 0.13[d]	1.50 ± 0.30[d]	1.80 ± 0.30[b]
$AnO_2^{2+} + Cl^- \rightleftarrows AnO_2Cl^+$	0.17 ± 0.02[c]	0.40 ± 0.17[d]	0.23 ± 0.03[d]
$AnO_2^{2+} + 2Cl^- \rightleftarrows AnO_2Cl_2(aq)$	−1.10 ± 0.40[d]	–	−1.15 ± 0.30[d]
$An^{4+} + Br^- \rightleftarrows AnBr^{3+}$	1.46 ± 0.20[d]	–	1.60 ± 0.30[d]
$An^{4+} + I^- \rightleftarrows AnI^{3+}$	1.25 ± 0.30[d]	1.50 ± 0.40[d]	–
$AnO_2^{2+} + IO_3^- \rightleftarrows AnO_2(IO_3)^{2+}$	2.00 ± 0.02[d]	1.20 ± 0.30[d]	–
$An^{4+} + NO_3^- \rightleftarrows AnNO_3^{3+}$	1.47 ± 0.13[d]	1.90 ± 0.15[d]	–
$An^{4+} + SO_4^{2-} \rightleftarrows An(SO_4)^{2+}$	6.58 ± 0.19[a]	6.85 ± 0.27[d]	6.89 ± 0.31[d]
$An^{4+} + 2SO_4^{2-} \rightleftarrows An(SO_4)_2(aq)$	10.51 ± 0.20[d]	11.05 ± 0.51[d]	11.14 ± 0.55[d]
$AnO_2^{2+} + SO_4^{2-} \rightleftarrows AnO_2(SO_4)(aq)$	3.15 ± 0.10[e]	3.28 ± 0.06[d]	3.38 ± 0.20[d]
$AnO_2^{2+} + 2SO_4^{2-} \rightleftarrows AnO_2(SO_4)_2^{2-}$	4.14 ± 0.15[e]	4.70 ± 0.10[d]	4.40 ± 0.20[d]
$An^{4+} + SCN^- \rightleftarrows AnSCN^{3+}$	2.97 ± 0.06[d]	3.00 ± 0.30[d]	–
$An^{4+} + 2SCN^- \rightleftarrows An(SCN)_2^{2+}$	4.26 ± 0.18[d]	4.10 ± 0.50[d]	–
$An^{4+} + 4CO_3^{2-} \rightleftarrows An(CO_3)_4^{4-}$	35.12 ± 0.96[d]	36.69 ± 1.03[b]	37.00 ± 1.10[d]
$An^{4+} + 5CO_3^{2-} \rightleftarrows An(CO_3)_5^{6-}$	34.00 ± 0.90[d]	35.62 ± 1.05[b]	35.65 ± 1.13[d]
$AnO_2^+ + 3CO_3^{2-} \rightleftarrows AnO_2(CO_3)_3^{5-}$	6.95 ± 0.36[d]	5.50 ± 0.07[d]	5.61 ± 0.24[e]
$AnO_2^{2+} + CO_3^{2-} \rightleftarrows AnO_2(CO_3)(aq)$	9.94 ± 0.03[d]	9.86 ± 0.10[e]	9.50 ± 0.50[d]
$AnO_2^{2+} + 2CO_3^{2-} \rightleftarrows AnO_2(CO_3)_2^{2-}$	16.61 ± 0.09[d]	16.52 ± 0.73[e]	14.70 ± 0.50[d]
$AnO_2^{2+} + 3CO_3^{2-} \rightleftarrows AnO_2(CO_3)_3^{4-}$	21.84 ± 0.04[d]	19.90 ± 0.50[e]	18.00 ± 0.50[d]
$2AnO_2^{2+} + CO_3^{2-} + 3H_2O \rightleftarrows (AnO_2)_2CO_3(OH)_3^- + 3H^+$	−0.86 ± 0.50[d]	−1.79 ± 1.92[e]	–
$3AnO_2^{2+} + 6CO_3^{2-} \rightleftarrows (AnO_2)_3(CO_3)_6^{6-}$	54.00 ± 1.00[d]	51.43 ± 2.14[e]	–

[a] Grenthe et al. (1992).
[b] Lemire et al. (2001).
[c] Aupiais et al. (2023).
[d] Guillaumont et al. (2003).
[e] Grenthe et al. (2020).

Table 2
Specific ion-interaction theory parameters used in this study.

Species	Counter-ion	U	Np	Pu
H^+	Cl^-	0.12 ± 0.01[a]		
Na^+	Cl^-	0.03 ± 0.01[a]		
HCO_3^-	Na^+	0.00 ± 0.02[a]		
CO_3^{2-}	Na^+	−0.08 ± 0.03[a]		
An^{4+}	Cl^-	–	–	–
AnO_2^+	Cl^-	–	0.09 ± 0.05[b]	–
AnO_2^{2+}	Cl^-	0.21 ± 0.02[a]	–	–
$An(OH)_4$ (aq)	$Na^+(Cl^-)$	0[h]	0[h]	0[h]
$An(CO_3)_4^{4-}$	Na^+	−0.09 ± 0.10[c]	–	–
$An(CO_3)_5^{6-}$	Na^+	−0.30 ± 0.15[c]	–	–
$AnO_2(CO_3)$(aq)	$Na^+(Cl^-)$	0[h]	0[h]	0[h]
$AnO_2(CO_3)_2^{2-}$	Na^+	−0.02 ± 0.09[c]	−0.02 ± 0.14[c]	−0.7 ± 0.2[b]
$AnO_2(CO_3)_3^{4-}$	Na^+	−0.01 ± 0.11[c]	−0.40 ± 0.19[c]	−0.2 ± 0.3[b]
$(AnO_2)_3(CO_3)_6^{6-}$	Na^+	0.37 ± 0.01[c]	−0.46 ± 0.73[c]	–
$(AnO_2)_2CO_3(OH)_3^-$	Na^+	0.00 ± 0.05[c]	–	–
$CaUO_2(CO_3)_3^{2-}$	$Na^+(Cl^-)$	0.29 ± 0.11[d]	–	–
	Na^+	0.12 ± 0.25[e]		
		−0.02 ± 0.09[f]		
$Ca_2UO_2(CO_3)_3$(aq)	$Na^+(Cl^-)$	0.66 ± 0.12[d]	–	–
		0.50 ± 0.38[e]		
		0[f]		
$MgUO_2(CO_3)_3^{2-}$	$Na^+(Cl^-)$	0.09 ± 0.16[g]	–	–
	Na^+	−0.02 ± 0.25[e]		
		−0.02 ± 0.09[f]		

[a] Grenthe et al. (1992).
[b] Lemire et al. (2001).
[c] Guillaumont et al. (2003).
[d] Shang and Reiller (2020).
[e] This study.
[f] Like-charged analogy to $\varepsilon(UO_2(CO_3)_2^{2-},Na^+) = -0.02 \pm 0.09$ kg_w mol^{-1} in Lee and Yun (2013) and in Thermochimie 11a.
[g] Shang and Reiller (2021a).
[h] By default.

difficult to apprehend as activities of Mg^{2+}, Ca^{2+}, HCO_3^-/CO_3^{2-}, Na^+, and H^+ have a direct impact. For uranium, Reiller and Descostes (2020) proposed $\log_{10}a(SO_4^{2-})$-pH at fixed $-\log_{10}a(Mg^{2+})$, $-\log_{10}a(Ca^{2+})$, and $-\log_{10}P(CO_2)$. Shang et al. (2023) proposed representations of activity products $\log_{10}(a(Ca^{2+})/a(H^+)^2)$–$\log_{10}(a(HCO_3^-)\ a(H^+))$–$\log_{10}(a(Na^+)/a(H^+))$. For the corresponding solids, Lee et al. (2019) also proposed the activity product $\log_{10}(a(Ca^{2+})\ a(HCO_3^-)^2)$. Jo et al. (2022) proposed a Pourbaix diagram for Pu at $[Ca]_{total} = 1$ mM and atmospheric $P(CO_2)$.

The influence of ionic strength on these species has been shown to be important, particularly on the globally neutral $Ca_2UO_2(CO_3)_3$(aq) complex. Shang and Reiller (2020) determined a non-nil value for $\varepsilon(Ca_2UO_2(CO_3)_3(aq),Na^+Cl^-) = 0.66$ kg_w mol^{-1}, contrary to generally accepted nil value for neutral complex — even if several neutral complexes have non-nil values in the literature (Ciavatta, 1980; Hummel et al., 2005; Plyasunova et al., 1998; Zhang and Muhammed, 2001), or ε values that can be calculated from $\Delta\varepsilon$ values (Brown and Ekberg, 2016; Powell et al., 2007, 2009, 2011). The like-charged hypothesis for $\varepsilon(Ae_nUO_2(CO_3)_3^{2-},Na^+)$ has also been questioned (Shang and Reiller, 2020, 2021a; Shang et al., 2020).

It is known since long that commonalities between similar elements can be represented through correlations (Irving and Rossotti, 1956) — namely linear free-energy relationships (LFERs) —, which could be used to estimate missing constants (Grenthe et al., 1997; Murphy and Shock, 1999) with an inevitable high uncertainty. It could be possible then to propose estimation of missing formation constants for $Ae_nAnO_2(CO_3)_3^{(4-2n)-}$, and to define their possible prevalence domain.

The purpose of the study, after comparison of existing literature values, is first to compare the prevalence domains of $Ae_nUO_2(CO_3)_3^{(4-2n)-}$ complexes in various relevant media based on selected values from NEA-OECD (Grenthe et al., 2020) and like-charged hypothesis for ε values (Lee and Yun, 2013), and on recent constants, functions of reaction and formation, and ε proposed from extrapolation to zero ionic strength of existing literature values. Second, based on these comparisons, LFERs for U–Pu, U–Np, and Pu–Np from NEA-OECD selections (Grenthe et al., 1992, 2020; Guillaumont et al., 2003; Lemire et al., 2001) will be plotted to estimate missing formation constants, and compare them to the sole existing determination (Jo et al., 2020). Finally, speciation (percent of species vs. pH or pe) and Pourbaix predominance diagram (E_h vs. pH) will be calculated to define the possible predominance domain and help orienting further studies.

2. Methods

2.1. General description

The formation of species ML from reactants M and L is described by the equilibrium thermodynamic law. Following Sillén and Martell (1964), the reaction constants can be written as follows, omitting charges for the sake of simplicity.

$$ML_{n-1} + L \rightleftarrows ML_n \quad K_n^\circ = \frac{[ML_n]}{[ML_{n-1}][L]} \tag{1}$$

$$M + nL \rightleftarrows ML_n \quad \beta_n^\circ = \frac{[ML_n]}{[M][L]^n} \tag{2}$$

Here, K°_n is a stepwise reaction constant, and β°_n a cumulative reaction constant.

The free energy of reaction is written as,

$$\Delta_r G_m^\circ = -RT \ln K_n^\circ \tag{3}$$

There are numerous compilation of thermodynamic functions and constants (Chase, 1998; Cox et al., 1989; Cross and Ewart, 1991; Grenthe et al., 1992, 2020; Guillaumont et al., 2003; Lemire et al., 2001; Naumov et al., 1974; Robie and Hemingway, 1995; Wagman et al., 1982), all of which are not always traceable (Hummel et al., 2019, and references therein).

For the actinides U, Np, and Pu, data have been selected by reviews commissioned by the TDB project from NEA-OECD (Grenthe et al., 1992, 2020; Guillaumont et al., 2003; Lemire et al., 2001) for ligands of interest for radioactive waste management programs, e.g., OH^-, F^-, SO_4^{2-}, PO_4^{3-}, CO_3^{2-}, H_4SiO_4(aq).

A general formation reaction of hydroxocarbonato complexes of uranyl (VI) is written as follows.

$$nUO_2^{2+} + mH_2O + pCO_3^{2-} \rightleftarrows (UO_2)_n(OH)_m(CO_3)_p^{(2n-m-2p)} + mH^+$$

$$\beta^\circ = \frac{a\left((UO_2)_n(OH)_m(CO_3)_p^{(2n-m-2p)}\right)\ a(H^+)^m}{a\left(UO_2^{2+}\right)^n\ a(H_2O)^m\ a\left(CO_3^{2-}\right)^p} \tag{4}$$

The general stepwise formation of $Ae_nAnO_2(CO_3)_3^{(4-2n)-}$ is written as follows,

$$Ae^{2+} + Ae_{n-1}UO_2(CO_3)_3^{(4-2(n-1))-} \rightleftarrows Ae_nUO_2(CO_3)_3^{(4-2n)-}$$

$$K_{n.1.3}^\circ = \frac{a\left(Ae_nAnO_2(CO_3)_3^{(4-2n)-}\right)}{a\left(Ae^{2+}\right)\ a\left(Ae_{n-1}AnO_2(CO_3)_3^{(4-2(n-1))-}\right)} \tag{5}$$

and the cumulative reaction is written as follows.

$$nAe^{2+} + UO_2^{2+} + 3CO_3^{2-} \rightleftarrows Ae_nUO_2(CO_3)_3^{(4-2n)-}$$

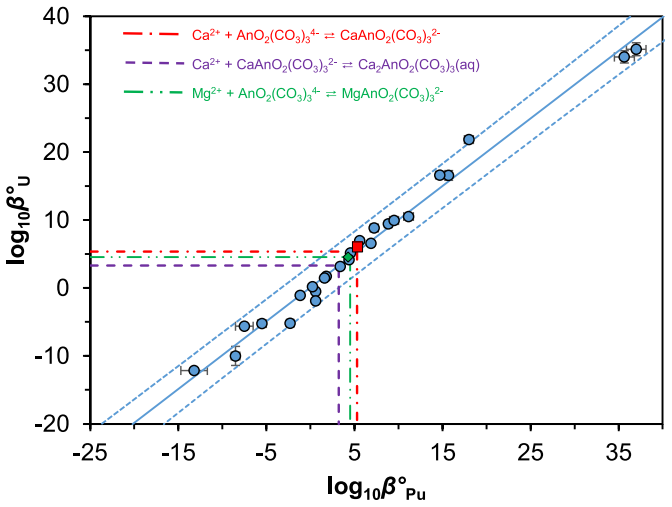

Fig. 1. Linear free energy relationship between uranium and plutonium inorganic species selected by the NEA-OECD TDB reviews (blue circles from Table 1, LFER blue line, uncertainty hyperboles short-dashed blue line); estimation of $\log_{10}K^{\circ}(CaPuO_2(CO_3)_3^{2-})$ (red dash-dotted line) and $\log_{10}K^{\circ}(Ca_2PuO_2(CO_3)_3(aq))$ (purple long-dashed line) and $\log_{10}K^{\circ}(MgPuO_2(CO_3)_3^{2-})$ (green double dot dashed line) from the LFER using $\log_{10}K^{\circ}$ from Shang and Reiller (2020) for Ca^{2+}, and Shang and Reiller (2021a) for Mg^{2+}; experimental value for $\log_{10}K^{\circ}(AePuO_2(CO_3)_3^{2-})$ (Mg green diamond, Ca red square) from Jo et al. (2020). (For interpretation of the references to colour in this figure legend, the reader is referred to the Web version of this article.)

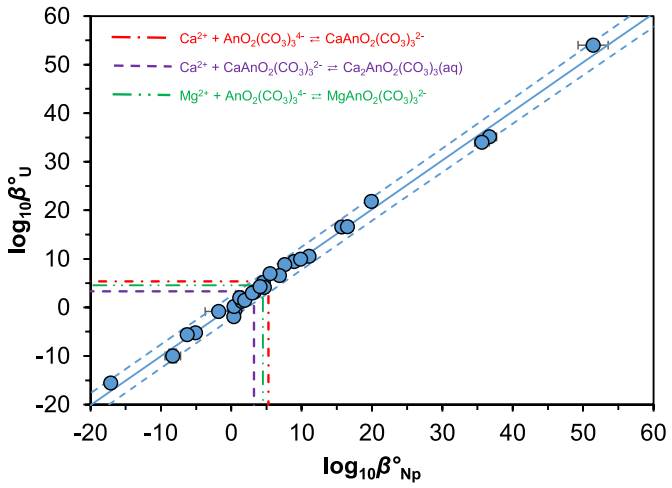

Fig. 2. Linear free energy relationship between uranium and neptunium inorganic species selected by the NEA-OECD TDB reviews (blue circles) from Table 1, LFER (blue line), uncertainty hyperboles (dashed blue line); estimation of $\log_{10}K^{\circ}(CaNpO_2(CO_3)_3^{2-})$ (red dash-dotted line) and $\log_{10}K^{\circ}(Ca_2NpO_2(CO_3)_3(aq))$ (purple dashed line) and $\log_{10}K^{\circ}(MgNpO_2(CO_3)_3^{2-})$ (green double dash dotted line) from the LFER using $\log_{10}K^{\circ}(Ae_nUO_2(CO_3)_3^{(4-2n)-})$ from Shang and Reiller (2020, 2021a). (For interpretation of the references to colour in this figure legend, the reader is referred to the Web version of this article.)

$$\beta^{\circ}_{n.1.3} = \frac{a\left((UO_2)_n(OH)_m(CO_3)_p^{(2n-m-2p)}\right)}{a\left(UO_2^{2+}\right)^n a\left(Ae^{2+}\right)^n a\left(CO_3^{2-}\right)^p} \quad (6)$$

The influence of ionic strength I_m on $\log_{10}K$ values is accounted for in the NEA-OECD reviews (Grenthe et al., 1992, 2020; Guillaumont et al., 2003; Lemire et al., 2001) through the specific ion-interaction theory (SIT),

$$\log_{10} K = \log_{10}K^{\circ} + \frac{A(T)\Delta z^2\sqrt{I_m}}{1+1.5\sqrt{I_m}} - \Delta\varepsilon\, I_m \quad (7)$$

where A (289.15 K) = 0.509 $kg_w^{½}$ $mol^{-½}$.

$$\Delta\varepsilon = \sum_i \nu_i\varepsilon_i \quad (8)$$

with ν_i the stoichiometric coefficient of species i — positive for products and negative for reactants —, and ε_i the specific ion-interaction parameter of species i tabulated in NEA-OECD reviews (Grenthe et al., 1992, 2020; Guillaumont et al., 2003; Lemire et al., 2001).

However, due to their selective nature, these compilations are intrinsically incomplete. It means that either thermodynamic functions ($\Delta_rG^{\circ}_m$, $\Delta_rH^{\circ}_m$, $\Delta_rS^{\circ}_m$), or constants ($\log_{10}K^{\circ}$ or $\log_{10}\beta^{\circ}$), or ε values are missing.

It has been observed since long that for similar complexes of analogous elements linear relationships exist between $\log_{10}K$, or $\log_{10}\beta$, values (Irving and Rossotti, 1956, and references therein) that are related to free energy — $\Delta_rG^{\circ}_m$/RTln(10), see eq. (3). These linear free energy relationships (LFERs) can be used to estimate missing data (Grenthe et al., 1997).

2.2. Linear free energy relationships

2.2.1. General thermochemical data and SIT parameters

For the LFERs between complexation constants, as stressed in Grenthe et al. (1997) *it is within classes of reactions that share some common characteristics that correlations are most precise*. Nevertheless, as we will see it afterwards, a certain level of precision can be attained even if

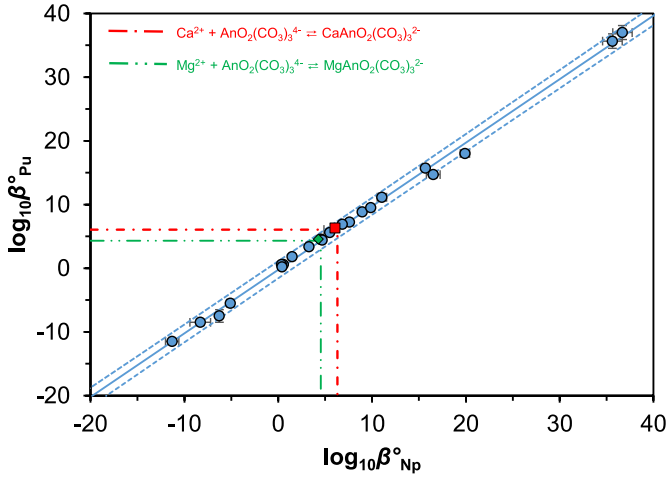

Fig. 3. Linear free energy relationship between plutonium and neptunium inorganic species selected by the NEA-OECD TDB reviews (blue circles) from Table 1, LFER (blue line), uncertainty hyperboles (dashed blue line); estimation of $\log_{10}K^{\circ}(CaNpO_2(CO_3)_3^{2-})$ (red dash-dotted line) and $\log_{10}K^{\circ}(MgNpO_2(CO_3)_3^{2-})$ (green double dash-dotted line) from the LFER using $\log_{10}K^{\circ}(AePuO_2(CO_3)_3^{2-})$ from Jo et al. (2020). (For interpretation of the references to colour in this figure legend, the reader is referred to the Web version of this article.)

Table 3
Regression parameters of the $\log_{10}\beta^{\circ}(U) = f(\log_{10}\beta^{\circ}(An))$.

	$\log_{10}\beta^{\circ}{}_U = f$ ($\log_{10}\beta^{\circ}{}_{Np}$)	$\log_{10}\beta^{\circ}{}_U = f$ ($\log_{10}\beta^{\circ}{}_{Pu}$)	$\log_{10}\beta^{\circ}{}_{Pu} = f$ ($\log_{10}\beta^{\circ}{}_{Np}$)
slope	1.008 ± 0.015	0.995 ± 0.026	0.998 ± 0.011
y-intercept	0.035 ± 0.238	0.073 ± 0.365	−0.248 ± 0.156
$S_{x/y}$	1.1283	1.5326	0.6251
r^2	0.9939	0.9840	0.9975
Degrees of freedom	27	23	20
$\bar{y} = \overline{\log_{10}\beta^{\circ}(U)}$	7.480	6.016	6.948
SSR ($\log_{10}\beta^{\circ}(An)$)	5549.05	3356.64	3139.87

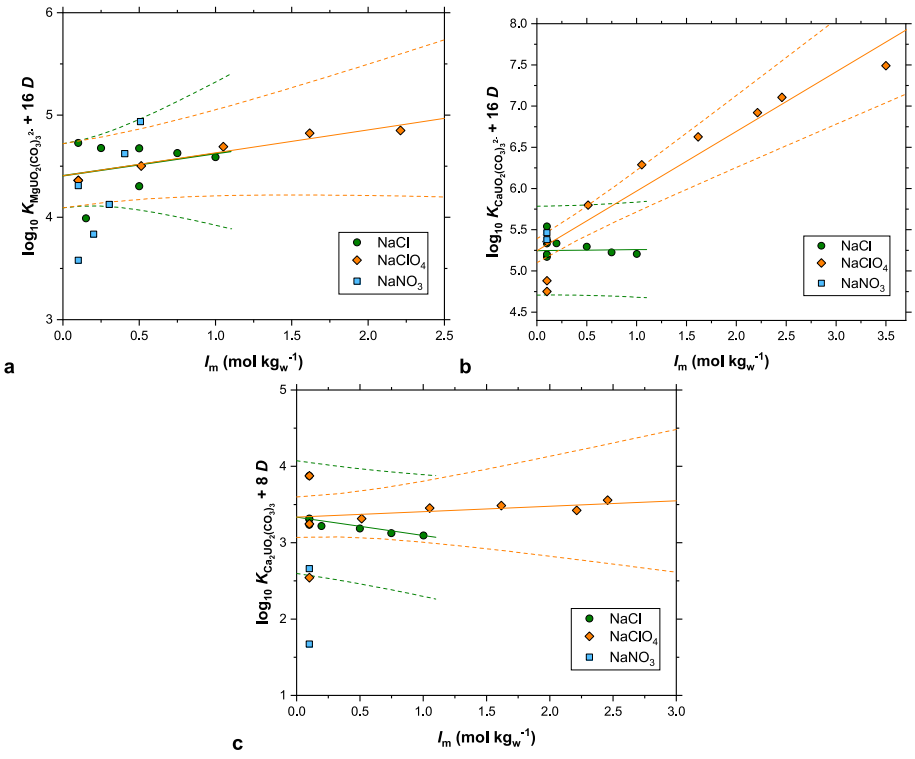

Fig. 4. SIT plot of the NaCl (green lines and circles), $NaClO_4$ (orange lines and diamonds) and $NaNO_3$ (blue squares) of the formation constant of $MgUO_2(CO_3)_3^{2-}$ (a), $CaUO_2(CO_3)_3^{2-}$ (b), and $Ca_2UO_2(CO_3)_3$(aq) (c) from Table S1 of the SI; plain lines are the linear fits and dashed lines are the propagations of errors (green for NaCl, orange for $NaClO_4$). (For interpretation of the references to colour in this figure legend, the reader is referred to the Web version of this article.)

either the ligands or the redox states of the metals are not totally the same.

The logarithm of the thermodynamic constants of the common complexes between U, Np, and Pu, are reported in Table 1. The ε parameters for the SIT, on which the effect of ionic strength on complexation constants is based (Grenthe et al., 2013) in the NEA-OECD reviews (Grenthe et al., 1992, 2020; Guillaumont et al., 2003; Lemire et al., 2001; Silva et al., 1995), are regrouped in Table 2. The value of $PuO_2(OH)$(aq) in Grenthe et al. (2020) was not included in Table 1, as it is an upper estimated value. The recent determination by Aupiais et al. (2023) was used instead, even if this estimation was done using like-charged analogy between $\varepsilon(NpO_2^+,Cl^-)$ and $\varepsilon(PuO_2^+,Cl^-)$, and $\varepsilon(PuO_2(OH)(aq),Na^+Cl^-) = 0$, the low 0.1 M ionic strength was inducing a low influence of $\Delta\varepsilon\, I_m$ in equation (7) — an estimation using equation from Davies (1962) gives the same value.

The LFERs $\log_{10}\beta^\circ(U) = f(\log_{10}\beta^\circ(An))$ are plotted in Figs. 1 and 2, for Pu and Np, respectively. The LFER $\log_{10}\beta^\circ(Pu) = f(\log_{10}\beta^\circ(Np))$ is plotted in Fig. 3. The regression parameters presented in Table 3 are used to draw the uncertainty hyperboles. It can be noted that: (i) the slopes between the $\log_{10}\beta^\circ$ values are not significantly different from unity and y-intercepts are not different from nil according to $2\sigma_y$; and (ii) that the values for the cumulative formations constants of $(AnO_2)_3(OH)_5^+$, $An(CO_3)_4^{4-}$, $An(CO_3)_5^{6-}$, and $(AnO_2)_3(CO_3)_6^{6-}$ are importantly driving the values of the slopes. The main difference between these elements is the redox potential values of the free ions (Vercouter, 2021; Vitorge, 1999) that are not accounted for in the LFERs.

The common enthalpy of reaction values for U–Pu and U–Np are too scarce to obtain a satisfying correlation: 2 values for U–Pu(IV), 5 for U–Pu(VI), 5 for U–Np(IV), 2 for U–Np(VI) in addition to the 4 pairs of redox species. If the enthalpies of formation are fairly well aligned (Fig. S1a of the SI), the $\Delta_f H^\circ_m$ ($Ae_nUO_2(CO_3)_3^{(4-2n)-}$) values are lower than the available values of the correlation and the uncertainties of $\Delta_r H^\circ_m$ correlations for Pu(VI) are too high (Fig. S1b of the SI).

2.2.2. *Reinterpretation of $Ae_nUO_2(CO_3)_3^{(4-2n)-}$ data from literature*

Since the seminal work from Bernhard et al. (1996), there have been several determinations of the formation constants of the $Ae_nUO_2(CO_3)_3^{(4-2n)-}$ complexes (Amayri, 2002; Bernhard et al., 2001; Dong and Brooks, 2006, 2008; Endrizzi and Rao, 2014; Geipel et al., 2008; Jo et al., 2019a, 2019b; Kalmykov and Choppin, 2000; Lee et al., 2017; Lee and Yun, 2013; Maia et al., 2021). Among them, some only identified the $Ca_2UO_2(CO_3)_3$(aq) complex (Bernhard et al., 1996; Kalmykov and Choppin, 2000) or only suggested the formation of $CaUO_2(CO_3)_3^{2-}$ (Bernhard et al., 2001). The effect of ionic strength on the repartition of species is important for these voluminous species, but the effect of this parameter was not studied often (Dong and Brooks, 2008; Kalmykov and Choppin, 2000; Shang and Reiller, 2020, 2021a, 2021b; Shang et al., 2020), or only postulated from like-charge comportment (Endrizzi and Rao, 2014; Lee and Yun, 2013). Following the original work from Bernhard et al. (1996), a large part of these studies were performed using the strong luminescence increase of $UO_2(CO_3)_3^{4-}$ with Ae^{2+} concentration in time-resolved laser-induced fluorescence spectroscopy (TRLFS). The luminescence of $Ae_nUO_2(CO_3)_3^{(4-2n)-}$ species, with $n = \{0, 1, 2\}$, have a distinctive blue shift relative to the free uranyl ion and slight shift between Mg and Ca species (Oher et al., 2020; Shang and Reiller, 2021a). Ion-exchange resins (Dong and Brooks, 2006, 2008; Maia et al., 2021), UV–Visible spectroscopy (Jo et al., 2019a, 2019b), Ca-selective electrode (Endrizzi and Rao, 2014; Jo et al., 2019b), or calorimetry (Endrizzi and Rao, 2014) were also used. A critical analysis of the data published before the cut-off date (2017) has been done in Grenthe et al. (2020). The different values of $\log_{10}K$ values are reported in Table S1 of the SI.

The interpretation in the framework of the SIT using equation (7) are shown in Fig. 4. The extrapolation of $\log_{10}K(AeUO_2(CO_3)_3^{(4-2n)-}) - \Delta z^2 D$ values were obtained in NaCl and $NaClO_4$ using multilinear fittings. The case of $NaNO_3$ was not treated with the NaCl and $NaClO_4$ media, because: (i) only data for $MgUO_2(CO_3)_3^{2-}$ vs. I are available; and (ii) the variation of values of $\log_{10}K(MgUO_2(CO_3)_3^{2-})$ vs. ionic strength of Dong

Table 4
Thermodynamic constants of $Ae_nAnO_2(CO_3)_3^{(4-2n)-}$ complexes, for An (VI) = {U(VI), Np(VI), Pu(VI)}; values in italic are from LFERs (Table 3).

Equilibrium	$\log_{10}K^\circ_{n.1n3}$ or $\log_{10}\beta^\circ_{n.1.3}$		
	U	Np	Pu
$Mg^{2+} + AnO_2(CO_3)_3^{4-} \rightleftarrows MgAnO_2(CO_3)_3^{2-}$	4.56 ± 0.09[a]	4.5 ± 1.1	4.5 ± 1.6
	4.36 ± 0.20[b]	4.3 ± 1.1	4.3 ± 1.6
	4.41 ± 0.11[c]	4.3 ± 1.1	4.4 ± 1.6
		4.5 ± 0.6	4.29 ± 0.18[d]
$Mg^{2+} + AnO_2^{2+} + 3CO_3^{2-} \rightleftarrows MgAnO_2(CO_3)_3^{2-}$	26.40 ± 0.09[a]	*24.4 ± 1.1*[g]	*22.5 ± 1.6*
	26.20 ± 0.20[b]	*24.2 ± 1.1*[g]	*22.3 ± 1.6*
	26.25 ± 0.12[c,g]	*24.2 ± 1.1*[g]	*22.4 ± 1.6*
		24.4 ± 0.8[g]	22.29 ± 1.61[d,g]
$Mg^{2+} + MgAnO_2(CO_3)_3^{2-} \rightleftarrows Mg_2AnO_2(CO_3)_3(aq)$	0.9 + 0.6[b]	*0.9 ± 1.1*	*0.9 ± 1.6*
$2Mg^{2+} + AnO_2(CO_3)_3^{4-} \rightleftarrows Mg_2AnO_2(CO_3)_3(aq)$	n.d.[a]		
	5.26 ± 0.60[b]	5.2 ± 1.1	5.1 ± 1.6
$2Mg^{2+} + AnO_2^{2+} + 3CO_3^{2-} \rightleftarrows Mg_2AnO_2(CO_3)_3(aq)$	n.d.[a]		
	27.10 + 0.60[b]	25.1 ± 1.1[g]	23.1 ± 1.6
$Ca^{2+} + AnO_2(CO_3)_3^{4-} \rightleftarrows CaAnO_2(CO_3)_3^{2-}$	5.36 ± 0.01[e]	5.3 ± 1.1	5.3 ± 1.6
	5.16 ± 0.20[b]	5.1 ± 1.1	5.1 ± 1.6
	5.25 ± 0.08[c]	5.2 ± 1.1	5.2 ± 1.6
		6.3 ± 0.6	6.05 ± 0.50[d]
$Ca^{2+} + AnO_2^{2+} + 3CO_3^{2-} \rightleftarrows CaAnO_2(CO_3)_3^{2-}$	27.20 ± 0.01[e,g]	*25.2 ± 1.1*[g]	*23.3 ± 1.6*[g]
	27.00 ± 0.20[b,g]	*25.0 ± 1.1*[g]	*23.1 ± 1.6*[g]
	27.09 ± 0.09[c,g]		*23.2 ± 1.6*[g]
		26.2 ± 0.8	24.05 ± 0.50[d]
$Ca^{2+} + CaAnO_2(CO_3)_3^{2-} \rightleftarrows Ca_2AnO_2(CO_3)_3(aq)$	3.29 ± 0.03[e]	*3.2 ± 1.1*	*3.2 ± 1.6*
	3.80 ± 0.35[b]	*3.7 ± 1.1*	*3.7 ± 1.6*
	3.33 ± 0.12[c]	*3.3 ± 1.1*	*3.3 ± 1.6*
$2Ca^{2+} + AnO_2(CO_3)_3^{4-} \rightleftarrows Ca_2AnO_2(CO_3)_3(aq)$			n.d.[d]
	8.65 ± 0.03[e]	8.5 ± 1.1	8.6 ± 1.6
	8.96 ± 0.40[b]	8.9 ± 1.1	8.9 ± 1.6
	8.58 + 0.14[c]	8.5 ± 1.1	8.5 ± 1.6
$2Ca^{2+} + AnO_2^{2+} + 3CO_3^{2-} \rightleftarrows Ca_2AnO_2(CO_3)_3(aq)$			n.d.[d]
	30.49 ± 0.03[e,g]	*28.4 ± 1.1*[g]	*26.6 ± 1.6*[g]
	30.80 ± 0.40[b,g]	*28.8 ± 1.1*[g]	*26.9 ± 1.6*[g]
	30.42 + 0.15[c]	*28.4 ± 1.1*[g]	*26.5 ± 1.6*[g]
$Sr^{2+} + AnO_2(CO_3)_3^{4-} \rightleftarrows SrAnO_2(CO_3)_3^{2-}$	4.06 ± 0.20[b]	4.0 ± 1.1	4.0 ± 1.6
	5.02 ± 0.01[f]		
$Sr^{2+} + AnO_2^{2+} + 3CO_3^{2-} \rightleftarrows SrAnO_2(CO_3)_3^{2-}$	25.90 ± 0.20[b,g]	23.9 ± 1.1[g]	22.0 ± 1.6[g]
	26.86 ± 0.04[f]		
$2Sr^{2+} + AnO_2(CO_3)_3^{4-} \rightleftarrows Sr_2AnO_2(CO_3)_3(aq)$	7.86 ± 0.50[b]	7.8 ± 1.1	7.8 ± 1.6
$2Sr^{2+} + AnO_2^{2+} + 3CO_3^{2-} \rightleftarrows Sr_2AnO_2(CO_3)_3(aq)$	29.70 + 0.50[g]	27.7 ± 1.1[g]	25.8 ± 1.6[g]
$Ba^{2+} + AnO_2(CO_3)_3^{4-} \rightleftarrows BaAnO_2(CO_3)_3^{2-}$	3.76 ± 0.30[b]	3.7 ± 1.1	3.7 ± 1.6
	4.84 ± 0.02[f]		
$Ba^{2+} + AnO_2^{2+} + 3CO_3^{2-} \rightleftarrows BaAnO_2(CO_3)_3^{2-}$	25.60 ± 0.30[b,g]	23.6 ± 1.1[g]	21.7 ± 1.6[g]
	26.68 ± 0.04[f,g]		

[a] Shang and Reiller (2021a).
[b] Grenthe et al. (2020).
[c] This study.
[d] Jo et al. (2020).
[e] Shang and Reiller (2020).
[f] Dong and Brooks (2006).
[g] $\log_{10}\beta^\circ = \log_{10}K^\circ + \log_{10}\beta^\circ(AnO_2(CO_3)_3^{4-})$; n. d. not detected.

and Brooks (2008) are quite important as seen in Fig. 4a, even compared to $\log_{10}K(CaUO_2(CO_3)_3^{2-})$ in $NaClO_4$ (Shang et al., 2020) and even to the value at 0.1 M (Dong and Brooks, 2006). As differences of comportment were evidenced between NaCl and $NaClO_4$ media (Shang and Reiller, 2020, 2021a; Shang et al., 2020), further works are needed to elucidate this comportment in $NaNO_3$ — particularly in view of the comments in Grenthe et al. (2020) that led to the non-selection of these data by the critical review.

Data for the formation of $Ae_nUO_2(CO_3)_3^{(4-2n)-}$ complexes and ε values either proposed in the literature, selected in the latter selection from the NEA-OECD (Grenthe et al., 2020), or determined here are reported in Tables 2 and 4. It can be seen that the obtained values are in agreement with estimation available otherwise. It is also noteworthy that even rejected in Grenthe et al. (2020), the data from Dong and Brooks (2006) are described satisfactorily by the extrapolations. The general comportment in ionic strength is inevitably mainly driven by the data from Shang et al. (Shang and Reiller, 2020, 2021a; Shang et al., 2020). Accounting for the other data is increasing the uncertainties, particularly the ones for $\Delta\varepsilon$ and $\varepsilon(Ae_nUO_2(CO_3)_3^{(4-2n)-}, Na^+X^-)$. Interestingly enough, given the large uncertainties on $\varepsilon(MgUO_2(CO_3)_3^{2-}, Na^+Cl^-)$, the value determined here is not significantly different from the like-charged hypothesis value with $\varepsilon(UO_2(CO_3)_2^{2-}, Na^+)$.

An estimation of the differences between the different values can be seen in Fig. S1 of the SI. The speciation of a 1 nmol kg_w^{-1} uranium solution at pH 8 containing 0.38 mol kg_w^{-1} NaCl, 0.01 mol kg_w^{-1} $CaCl_2$, and 0.05 mol kg_w^{-1} $MgCl_2$, and 2 mmol kg_w^{-1} $NaHCO_3$ — $I_m = 0.54$ mol kg_w^{-1} — gives a marked difference between results from Thermochimie 11a on the one hand, and Shang and Reiller (2020, 2021a) or estimation in Tables 2 and 4 on the other hand. This difference can be mainly attributed to the highest value of $\log_{10}\beta^\circ(Ca_2UO_2(CO_3)_3(aq))$ in Grenthe et al. (2020). The influence of the ε values will be evidenced in the following.

From the very small differences between the values from Shang and Reiller (2020, 2021a) or estimation in Tables 2 and 4, and for the sake of coherency in the data, the former values will be used in the following.

2.2.3. $\log_{10}K^\circ$ over ionic radius relationship

An interesting and complementary way to represent the variation of

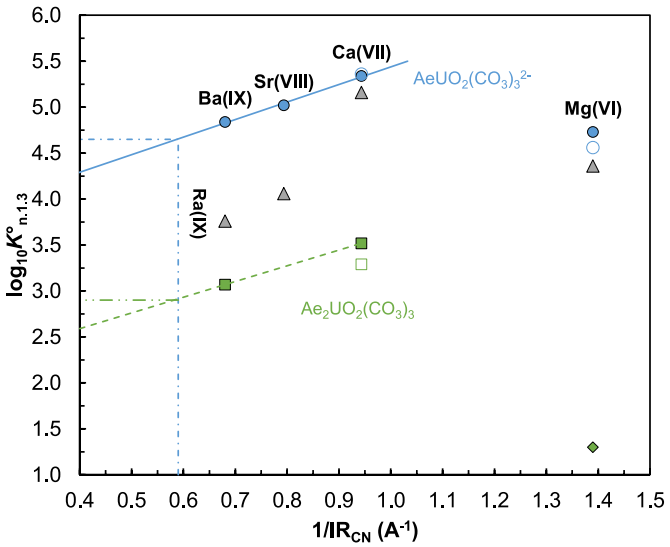

Fig. 5. $\log_{10}K^{\circ}(Ae_nUO_2(CO_3)_3^{(4-2n)-})$ vs. $1/IR_{CN}$ (Brackett et al., 1963; Kerisit and Liu, 2010) — n = 1 (circles), and n = 2 (squares, diamond, and triangles) — from Dong and Brooks (2006) (filled circles and squares), Grenthe et al. (2020) (filled triangles), Shang and Reiller (Shang and Reiller, 2020, 2021a) (empty circles and squares), and Jo et al. (2019a) (filled diamond): plain blue line is the linear relationship $1/IR_{CN} = f(\log_{10}K^{\circ}_{n.1.3})$ for Ca, Sr, and Ba from Dong and Brooks (2006); green dotted line is the linear relationship between Ca and Ba from Dong and Brooks (2006); the blue dotted and dash-dot lines are the estimation of a potential $\log_{10}K^{\circ}(RaUO_2(CO_3)_3^{2-})$ complex considering IR_{VIII} or IR_{IX}, respectively; the green long dash-dot and dash-dot-dot lines are the estimation of a potential $\log_{10}K^{\circ}(Ra_2UO_2(CO_3)_3(aq))$ complex considering IR_{VIII} or IR_{IX}, respectively. (For interpretation of the references to colour in this figure legend, the reader is referred to the Web version of this article.)

$\log_{10}K^{\circ}$ values for common charged central ion is vs. the charge over the distance between the metal and the ligand (z/r) (Grenthe et al., 1997; Kossiakoff and Harker, 1938). For the same metal type and charge, and ligand, it can be plotted vs. the inverse of effective ionic radii IR_{CN} (Shannon, 1976) (Fig. 5 and Table S2 of the SI), where the coordination numbers (CN) are taken from Kerisit and Liu (2010) for Mg^{2+} (IR_{VI} = 0.72 Å), Ca^{2+} (IR_{VII} = 1.06 Å), and Sr^{2+} (IR_{VIII} = 1.26 Å), and IR_{IX} = 1.47 Å from Ba^{2+} coordination in halides (Brackett et al., 1963). It appears that the $\log_{10}K^{\circ}(AeUO_2(CO_3)_3^{2-})$ values for Ca^{2+}, Sr^{2+}, and Ba^{2+} from Dong and Brooks (2006) and Shang and Reiller (2020) are following a linear relationship, and that octaedral Mg^{2+} is out of this trend for symmetry reasons hypothesized in details in Shang and Reiller (2021a). The $\log_{10}K^{\circ}(Ae_2UO_2(CO_3)_3(aq))$ values for Ca^{2+} and Ba^{2+} from Dong and Brooks (2006) and Shang and Reiller (2021a) seem to follow a linear relationship as well, with the $\log_{10}K^{\circ}(Mg_2UO_2(CO_3)_3(aq))$ value form Lee et al. (2017) out of the trend, for the same reasons — see discussions in Shang and Reiller (2021a). The selected data from Grenthe et al. (2020), also plotted in Fig. 5, seem to follow the same trend but with Ca, Sr, and Ba having a different slope. It is noteworthy that the values of Sr and Ba used to obtain the selection, in addition to the values from Dong and Brooks (2006), are linked to values obtained in $NaClO_4$ where the KCl electrode filling of the pH-electrode seemed not to have been replaced — see Shang et al. (2020) and Shang and Reiller (2021a).

A linear regression $1/IR_{CN}$ vs. $\log_{10}K^{\circ}_{1.1.3}$ (Neuilly, 1998) — and not $\log_{10}K^{\circ}_{1.1.3}$ vs. $1/IR_{CN}$ as classically plotted in Fig. 5 — allows estimating a potential $\log_{10}K^{\circ}(RaUO_2(CO_3)_3^{2-})$ (Table S3 of the SI). The CN value of Ra is not straightforwardly estimated. Knowing the propensity of Ra^{2+} to form homogeneous solid solution with Ba^{2+} in sulphate medium (Curti et al., 2010; Lestini et al., 2019), the values for Ra_{IX} could be seen as more likely. A calculation using IR_{IX} = 1.70 Å for Ra^{2+} turn into $\log_{10}K^{\circ}(RaUO_2(CO_3)_3^{2-}) = 4.6 \pm 0.9$ or $\log_{10}\beta^{\circ}(RaUO_2(CO_3)_3^{2-}) = 26.5 \pm 1.0$ (Table S2 of the SI).

A conservative similar estimation for a potential $Ra_2UO_2(CO_3)_3(aq)$ complex from the only $\log_{10}K^{\circ}(Ca_2UO_2(CO_3)_3(aq))$ and $\log_{10}K^{\circ}(Ba_2UO_2(CO_3)_3(aq))$ values from Table S3 of the SI — $Mg_2UO_2(CO_3)_3(aq)$ is not taken into account (vide supra) — gives $\log_{10}K^{\circ}(Ra_2UO_2(CO_3)_3(aq)) = 3.0$, or $\log_{10}\beta^{\circ}(Ra_2UO_2(CO_3)_3(aq)) = 29.5$ (Table S2 of the SI) — no standard deviation can be calculated.

From the usual radium concentration in natural waters, or even in water related to mining activities, the formation of the $Ra_nUO_2(CO_3)_3^{(4-2n)-}$ complexes is not likely to impact the speciation of both uranium(VI) and radium(II).

2.3. Speciation

All speciation calculations in the following were done using PhreeqC 3.5.7–15968 (Parkhurst and Appelo, 1999, 2013) or Phreeplot (Kinniburgh and Cooper, 2011). Database files used were the Thermochimie 11a (Giffaut et al., 2014; Grivé et al., 2015) (https://www.thermochimie-tdb.com/), and the Prodata 1.5.3.1 extractions (Reiller, 2022; Reiller and Descostes, 2020) — it can be noted that Thermochimie 12a issued October 4, 2023, is not changing anything for Ca–U(VI)–CO_3 species. Both are centred on NEA-OECD selected data for uranium, but the latter does not include transuranium elements. In both database extraction files, actinide data are mostly based on the NEA-OECD selected data (Grenthe et al., 1992, 2020; Guillaumont et al., 2003; Lemire et al., 2001; Silva et al., 1995). Some complementary data are to be noted straightforwardly, as the inclusion of $An(OH)_2(CO_3)_2^{2-}$ (Rai et al., 1999a, 1999b) in Thermochimie 11a to represent the increase of AnO_2 solubility vs. carbonate concentration — Yamaguchi et al. (1994) also proposed $Pu(OH)_4(CO_3)_2^{4-}$. The solubility of AnO_2 amorphous hydrated phases, noted AnO_2(am,hyd) in Grenthe et al. (2020), are written in Thermochimie 11a,

$$AnO_2{:}2H_2O + 4H^+ \rightleftarrows An^{4+} + 4H_2O$$

which does not change $\log_{10}K_s^{\circ}$ values, but maybe submitted to a stronger influence of water activity with increasing ionic strength.

The same remark applies to $PuO_2(OH)_2{:}H_2O$(am), noted $PuO_2(OH)_2$(am,hyd) in Grenthe et al. (2020).

Other complexes are included in Thermochimie 11a such as $Np(OH)_2^+$ (Allard et al., 1980) and $Pu(OH)_2^+$ in analogy to Am(III). These species will be of very little importance here.

In Thermochimie 11a, the $\varepsilon(AeUO_2(CO_3)_3^{2-},Na^+)$ values were from the like-charged hypothesis (Lee and Yun, 2013). In Prodata 1.5.3.1, $\log_{10}\beta^{\circ}$, $\Delta_r H^{\circ}_m$, and $\varepsilon(Ae_nUO_2(CO_3)_3^{(4-2n)-},Na^+Cl^-)$ from Shang and Reiller (2020, 2021a, b) were included.

3. Results and discussions

3.1. Uranium

Thermodynamic functions in Grenthe et al. (2020) allows calculating the oxidation potential diagram in Fig. 6 — it can be noted that $U(OH)^{3+}$ is ca. 2% at pH = 0 in $HClO_4$.

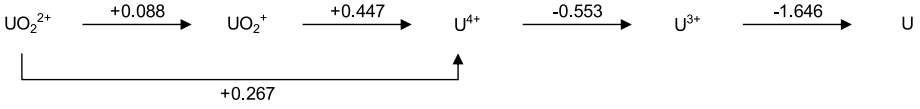

Fig. 6. The formal oxidation potential (Volt) diagram of uranium in acidic aqueous solutions (Grenthe et al., 2020).

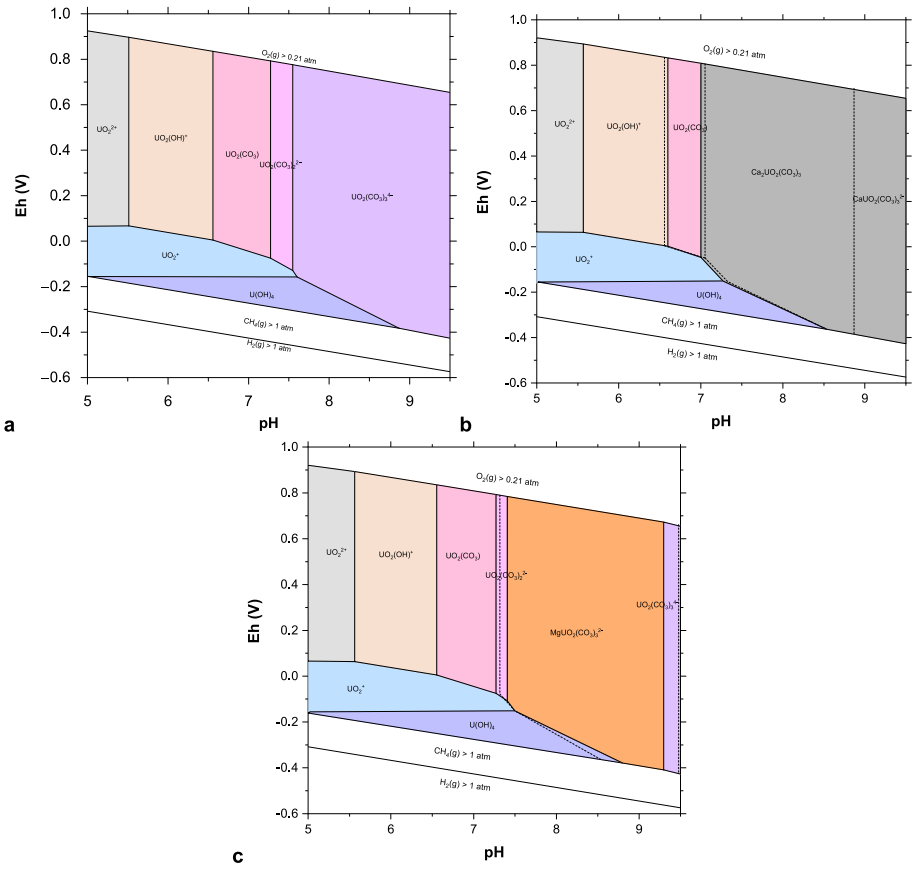

Fig. 7. Pourbaix diagrams (Kinniburgh and Cooper, 2011) of [U] = 0.1 nmol kg_w^{-1}, I_m = 0.1 mol kg^{-1} NaCl, and $P(CO_2) = 10^{-3.5}$ atm (Grenthe et al., 2020); considering no $Ae_nUO_2(CO_3)_3^{(4-2n)-}$ complexes (a), only the $Ca_nUO_2(CO_3)_3^{(4-2n)-}$ (b), or only the $MgUO_2(CO_3)_3^{2-}$ (c) complexes from NEA-OECD (plain line) or from Shang and Reiller (2020, 2021a) (b, c, dashed line); [Ae] = 5 mmol kg_w^{-1} — Ae is Ca (b) or Mg (c) —; no precipitation required.

3.1.1. *Impact of the origin of the data of $Ae_nUO_2(CO_3)_3^{(4-2n)-}$*

3.1.1.1. Case of Mg^{2+} and Ca^{2+}. Pourbaix (E_h vs. pH) predominance diagrams in Fig. 7 are obtained using either: (i) data from Grenthe et al. (2020) (Fig. 7a); (ii) $\log_{10}\beta^\circ(Ae_nUO_2(CO_3)_3^{(4-2n)-})$ from Grenthe et al. (2020) (Fig. 7b and c plain line) and $\varepsilon(AeUO_2(CO_3)_3^{2-},Na^+)$ from like-charged analogy (Lee and Yun, 2013) in Thermochimie 11a; and (iii) using $\log_{10}\beta^\circ(Ae_nUO_2(CO_3)_3^{(4-2n)-})$ and $\varepsilon(Ae_nUO_2(CO_3)_3^{(4-2n)-}, Na^+Cl^-)$ from Shang and Reiller (2020, 2021a) (Fig. 7b and c, dashed line). One can also note that no precipitation was required during calculation. Oversaturation of calcite ($CaCO_3$), magnesite ($MgCO_3$) or dolomite ($MgCa(CO_3)_2$) would reduce the predominance domains of the $Ae_nUO_2(CO_3)_3^{(4-2n)-}$ complexes. The differences between the $\log_{10}\beta^\circ(Ae_nUO_2(CO_3)_3^{2-})$ are evidenced in Fig. 7b and c. The lower $\log_{10}\beta^\circ(Ca_2UO_2(CO_3)_3(aq))$ value for Shang and Reiller (2020) induces a slightly larger prevalence domain of $UO_2(CO_3)(aq)$ complex and slightly greater prevalence domain of $Ca_2UO_2(CO_3)_3(aq)$. The higher values of $\log_{10}\beta^\circ$ and ε for Mg explains the larger predominance domain using the data from Shang and Reiller (2021a). The main difference comes from the values $\log_{10}\beta^\circ$ and ε from Shang and Reiller (2020) that induce the

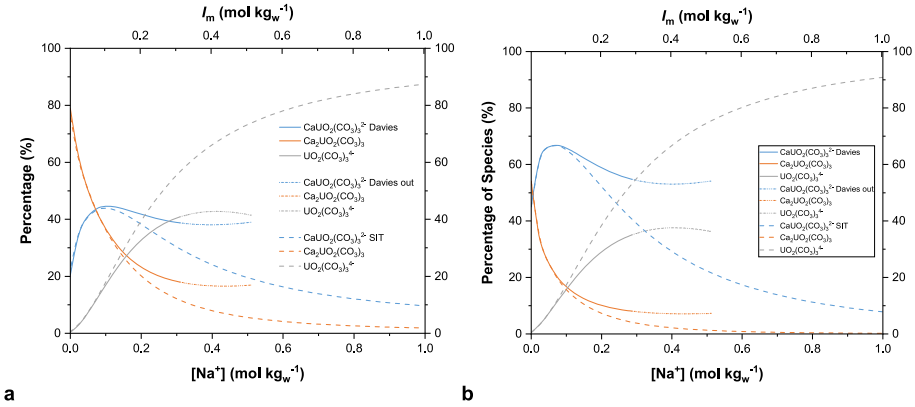

Fig. 8. Influence of NaCl concentration on 1 nmol kg_w^{-1} uranium speciation at pH = 8.1, $[Ca]_{tot}$ = 1 mmol kg_w^{-1}, and $P(CO_2) = 10^{-3.5}$ atm using thermochemical data in Table 1, and the $\log_{10}\beta^\circ(Ca_nUO_2(CO_3)_3^{(4-2n)-})$ values in Table 4 from NEA-OECD (used in Thermochimie 11a) (a) and Shang and Reiller (2020) (b): ionic strength corrections are Davies (1962) equation in the validity domain (plain line) and up to sea water domain (dotted line), and using the SIT $\varepsilon(Ca_nUO_2(CO_3)_3^{(4-2n)-},Na^+Cl^-)$ parameters (Table 2) from Lee and Yun (2013) in Thermochimie 11a (a) and Shang and Reiller (2020) (b) (dashed line).

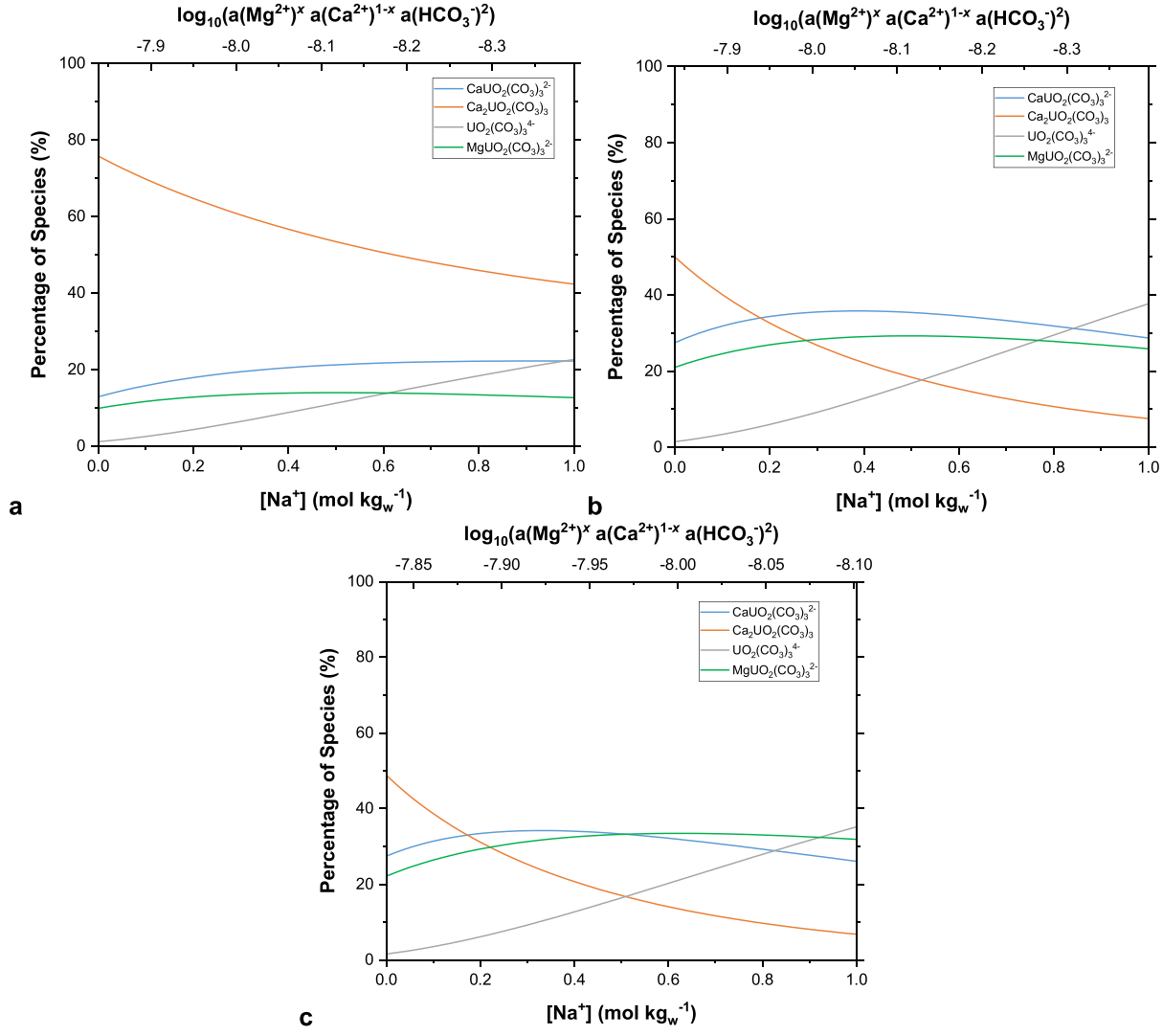

Fig. 9. Influence of Na^+ concentration on 1 nmol kg_w^{-1} uranium speciation at pH = 8.1 t = 25 °C, $[Mg]_{tot}$ = 54.7 mmol kg_w^{-1}, $[Ca]_{tot}$ = 10.6 mmol kg_w^{-1}, $[CO_3]_{total}$ = 2 mmol kg_w^{-1} — adapted from Millero et al. (2008) —, and $[Cl^-]$ from charge balance; thermochemical data are from Table 1 (in Thermochimie 11a) (a) implemented by the $\log_{10}\beta^\circ(Ae_nUO_2(CO_3)_3^{(4-2n)-})$ values from Shang and Reiller (Shang and Reiller, 2020, 2021a) (b), and Prodata 1.5.3.1 (Reiller, 2022) (c): ionic strength corrections using the SIT with $\varepsilon(Ae_nUO_2(CO_3)_3^{(4-2n)-},Na^+Cl^-)$ parameters from Thermochimie 11a (a), implemented with Shang and Reiller (2020, 2021a) (b), and Prodata 1.5.3.1 (Reiller, 2022) (c).

predominance of $CaUO_2(CO_3)_3^{2-}$ at pH > 8.87, due to the increase of Na^+ concentration, and thus ionic strength, during calculation in Phreeplot.

3.1.1.2. Case of Sr^{2+}, Ba^{2+}, and Ra^{2+}. The eventual impact of the other $Ae_nUO_2(CO_3)_3^{(4-2n)-}$ complexes, i.e., Sr^{2+}, Ba^{2+}, and Ra^{2+}, can be done using the solution ES-85 from Bellezane, France, which PHREEQC script is available in the Supplementary Information. It presented the highest carbonate concentration — or highest activity product $a(HCO_3^-)\ a(H^+) = 10^{-8.41}\ mol^2\ kg_w^{-2}$ — of the tested radium containing waters in Reiller and Descostes (2020). The speciation are reported in Table S4 of the SI, using only the Prodata 1.5.3.1 file — containing $SrUO_2(CO_3)_3^{2-}$, $BaUO_2(CO_3)_3^{2-}$, and $Ba_2UO_2(CO_3)_3$ from Dong and Brooks (2006) —, and implementing the $\log_{10}\beta^\circ(Ra_nUO_2(CO_3)_3^{(4-2n)-})$ in the PhreeqC input file.

It can be seen that only a mere fraction of total Ba, Ca, Mg, Sr, and Ra is engaged in a complexation with $Ae_nUO_2(CO_3)_3^{(4-2n)-}$. As already reported, uranium is controlled by $Ca_nUO_2(CO_3)_3^{(4-2n)-}$, but the calculated amount of $MgUO_2(CO_3)_3^{2-}$ is higher than in Reiller and Descostes (2020) (Fig. S3 of the SI), due to the implementation of the $\log_{10}\beta^\circ$ and ε from Shang et al. (Shang and Reiller, 2020, 2021a, 2021b; Shang et al., 2020).

Due to the differences in $\log_{10}\beta^\circ$ between Ca^{2+} and the other Ae^{2+} cations, higher total concentrations of Ae — or rather higher Ae^{2+} activities — are needed as underlined in Shang et al. (2023).

Even if potentially existing, the constant between the Ca and other Ae species can be calculated as follows.

$$CaUO_2(CO_3)_3^{2-} + Ae^{2+} \rightleftarrows AeUO_2(CO_3)_3^{2-} + Ca^{2+}$$

$$K^\circ = \frac{K^\circ\left(AeUO_2(CO_3)_3^{2-}\right)}{K^\circ\left(CaUO_2(CO_3)_3^{2-}\right)} = \frac{a\left(AeUO_2(CO_3)_3^{2-}\right)\ a\left(Ca^{2+}\right)}{a\left(CaUO_2(CO_3)_3^{2-}\right)\ a\left(Ae^{2+}\right)} = \frac{10^{\log_{10}K^\circ_{1.n.3}}}{10^{5.36}} \quad (9)$$

As all $\log_{10}K^\circ(Ae_nUO_2(CO_3)_3^{2-})$ or $\log_{10}\beta^\circ(Ae_nUO_2(CO_3)_3^{2-})$ other than Ca^{2+} are either lower, or awaited to be lower, than $CaUO_2(CO_3)_3^{2-}$, it comes out that a higher Ae concentration than Ca — or rather a higher Ae^{2+} activity than Ca^{2+} — is needed in natural waters, which can occur for Mg^{2+} (vide post) but is not likely for Sr^{2+}, Ba^{2+}, and Ra^{2+}.

3.1.2. Ionic strength evolution

3.1.2.1. NaCl concentration. In recent studies (Shang and Reiller, 2020,

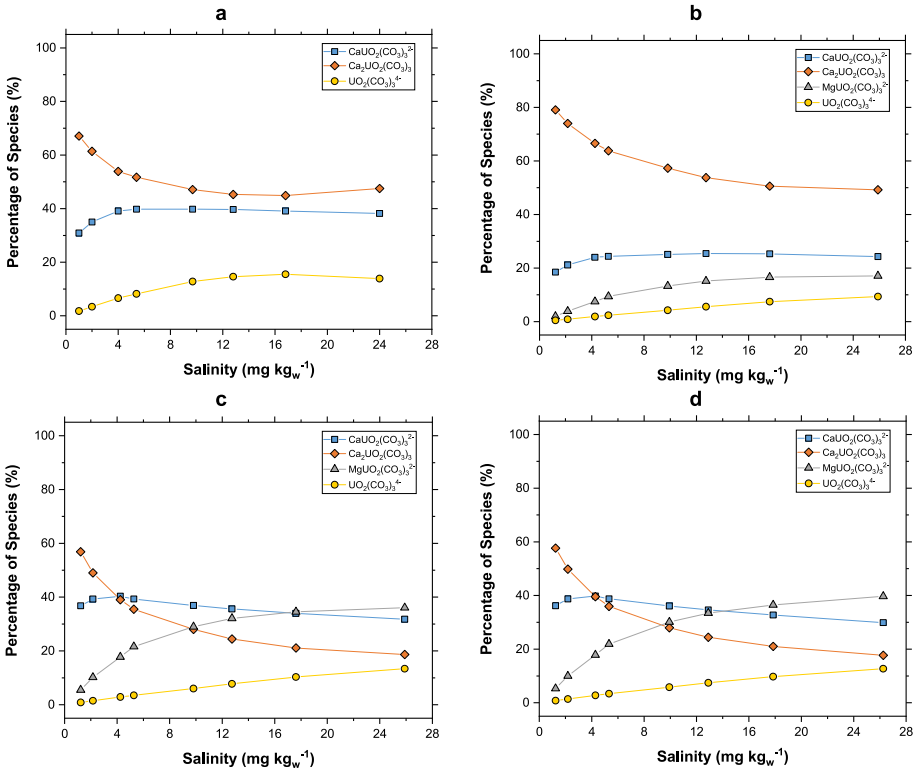

Fig. 10. Evolution of uranium speciation vs. salinity in the Scheldt estuary digitized from Fig. 6 and Table S3 in Smolíková et al. (2022) (a), calculated using NEA-OECD data (Grenthe et al., 2020, in Thermochimie 11a) (b), implemented with data from Shang and Reiller (2020, 2021a, b) (c), and using Prodata 1.5.3.1 database (d).

2021a; Shang et al., 2020) it was shown that the like-charged comportment in ionic strength for the $Ae_nUO_2(CO_3)_3^{(4-2n)-}$ complexes did not fully apply. The differences in speciation are shown for Thermochimie 11a (Fig. 8a), and implemented in the input file with $\log_{10}\beta^\circ(Ca_nUO_2(CO_3)_3^{(4-2n)-})$ and $\varepsilon(Ca_nUO_2(CO_3)_3^{(4-2n)-},Na^+Cl^-)$ from Shang and Reiller (2020) (Fig. 8b). In the validity domain of the Davies (1962) equation, the speciation is different because the $\log_{10}\beta^\circ$ value are favouring $Ca_2UO_2(CO_3)_3$(aq) for NEA-OECD (see Table 1). In both cases, the Davies (1962) equation deviates from the SIT speciation above 0.1 mol kg$_w^{-1}$, and speciation is substantially different: $CaUO_2(CO_3)_3^{2-}$ and $UO_2(CO_3)_3^{4-}$ are equally important with $Ca_2UO_2(CO_3)_3$(aq) as secondary species using NEA-OECD data in Thermochimie 11a ca. 0.3 mol kg$_w^{-1}$, when $CaUO_2(CO_3)_3^{2-}$ is dominant with Shang and Reiller (2020); $UO_2(CO_3)_3^{4-}$ is dominating the SIT calculation in both cases at $I_m > 0.3$ mol kg$_w^{-1}$.

It can thus be seen that, in general and for these complexes in particular, using an ionic strength correction beyond its validity domain is leading to important differences in calculated speciation. It also shows the importance of ε values in these cases. This was already cited as a limiting factor of speciation calculation by Nordstrom et al. (1979).

3.1.2.2. Case of sea water. A particular application of the ionic strength influence is the seawater. One must keep in mind the opening remarks in the discussion paragraph of Nordstrom et al. (1979). Even if the specific interaction theory has brought many advances, many comments are still true today.

The predominance of $Ca_2UO_2(CO_3)_3$(aq) was proposed based on either like-charged hypothesis for $\varepsilon(CaUO_2(CO_3)_3^{2-},Na^+) = \varepsilon(UO_2(CO_3)_2^{2-},Na^+)$ and $\varepsilon(Ca_2UO_2(CO_3)_3(aq),Na^+Cl^-) = 0$, or application of an ionic strength out of its domain — see Shang and Reiller (2020) Shang and Reiller (2021a) and references therein. Reiller and Descostes (2020) evidenced the need of further determination based on pre-existing values, to which the works from Shang et al. (Shang and Reiller, 2020, 2021a; Shang et al., 2020) answered. To further exemplify this, the calculated speciation of $Ae_nUO_2(CO_3)_3^{(4-2n)-}$ in solution adapted from seawater composition from Millero et al. (2008), also analysed in Reiller and Descostes (2020), is presented in Fig. 9 — one must note that boron chemistry is not included in Prodata 1.5.3.1. The $[Na]_{total}$ is varied from 0 to 1 mol kg$_w^{-1}$ starting from pH = 8.1, $[Ca]_{total}$ = 10.6 mmol kg$_w^{-1}$, $[Mg]_{total}$ = 54.7 mmol kg$_w^{-1}$, $[CO_3]_{total}$ = 2 mmol kg$_w^{-1}$, and $[Cl]_{total}$ concentration adjusted to charge balance, *i.e.*, from 0.13 to 1.13 mol kg$_w^{-1}$. The $[U]_{total}$ is fixed at 1 nmol kg$_w^{-1}$. Ionic strength is then varied between I_m = 0.19–1.18 mol kg$_w^{-1}$. The differences between the speciation from thermodynamic data and SIT parameters in Thermochimie 11a and Shang and Reiller (2020, 2021a) for $Ae_nUO_2(CO_3)_3^{(4-2n)-}$ are coming from: (i) the $\log_{10}\beta^\circ$ values favouring $Ca_2UO_2(CO_3)_3$(aq) using NEA-OECD (Thermochimie 11a) (Fig. 9a); and (ii) from the ε values gradually favouring $AeUO_2(CO_3)_3^{2-}$ using Shang and Reiller (2020, 2021a). The influence of the inclusion of $Na(HCO_3)$(aq) and $Na(CO_3)^-$ in Thermochimie 11a — even using the SIT extraction of the database in which they should not be present — on the proportion of $MgUO_2(CO_3)_3^{2-}$ vs. $Ca_nUO_2(CO_3)_3^{2-}$ is shown by comparison with the same calculation using the Prodata 1.5.3.1 database (Reiller, 2022; Reiller and Descostes, 2020).

Shang et al. (2023) identified that the proportion x of the sum of activities of Mg^{2+} and Ca^{2+} is directly impacting the predominance of $Ca_nUO_2(CO_3)_3^{(4-2n)-}$ and $MgUO_2(CO_3)_3^{2-}$ — and potentially $Mg_2UO_2(CO_3)_3$(aq).

$$x = \frac{a(Mg^{2+})}{a(Mg^{2+}) + a(Ca^{2+})} \quad (10)$$

It can be seen on the second x-axis in Fig. 9 that the activity product $a(Mg^{2+})^x\, a(Ca^{2+})^{1-x}\, a(HCO_3^-)^2$ is lower using Thermochimie 11a database for the same $[Na]_{total}$ in the solution — mostly due to the gradual increase of $Na(HCO_3)$(aq) concentrations —, which gradually favours $CaUO_2(CO_3)_3^{2-}$ vs. $MgUO_2(CO_3)_3^{2-}$ using Prodata 1.5.3.1 (Reiller, 2022;

Table 5
Thermodynamic function of formation for species implied in the pyrite/siderite (FeS_2/$FeCO_3$) redox buffer.

Species	$\Delta_f G°_m$ (kJ mol^{-1})	$\Delta_f H°_m$ (kJ mol^{-1})	Reference
O_2(g)	0	0	Grenthe et al. (2020)
H_2(g)	0	0	Grenthe et al. (2020)
H^+	0	0	Grenthe et al. (2020)
H_2O	−237.140 ± 0.041	−285.830 ± 0.040	Grenthe et al. (2020)
SO_4^{2-}	−744.004 ± 0.418	−909.340 ± 0.400	Grenthe et al. (2020)
CO_2(g)	−394.373 ± 0.133	−393.510 ± 0.130	Grenthe et al. (2020)
CO_3^{2-}	−527.900 ± 0.390	−675.230 ± 0.250	Grenthe et al. (2020)
FeS_2-pyrite (cr)	−162.219 ± 2.361	−173.630 ± 2.360	Lemire et al. (2013)
$FeCO_3$(cr)	−679.557 ± 0.917	−752.609 ± 0.895	Lemire et al. (2020)

Shang and Reiller, 2020).

Here again, it can be seen that the speciation of uranium is changed from a dominating neutral species (Fig. 9a) to the shared predominance with $AeUO_2(CO_3)_3^{2-}$ (Fig. 9b and c) depending on the $\varepsilon(AeUO_2(CO_3)_3^{2-}, Na^+)$ values.

3.1.2.3. Case of an estuary. A further interesting application of these data is the representation of the uranium speciation in an estuary where salinity *S* and concentration of carbonate, magnesium and calcium are gradually changing. Very recently, Smolíková et al. (2022) reported the evolution of the uranium speciation in the Scheldt Estuary (border between Belgium and The Netherlands). Uranium concentration was followed between Antwerp and the North Sea-ward. The authors calculated the speciation using Visual Minteq (https://vminteq.lwr.kth.se/) including the $Ca_nUO_2(CO_3)_3^{(4-2n)-}$ data from Dong and Brooks (2006) — i.e. with no SIT parameters, and $MgUO_2(CO_3)_3^{2-}$ apparently not included —, and the very minor natural organic matter influence. The speciation was suggesting that $Ca_2UO_2(CO_3)_3$(aq) was dominating whatever the salinity *S* — increasing from Antwerp to the sea-ward — and that $UO_2(CO_3)_3^{4-}$ percentage was increasing with *S* (Fig. 10a) — Fig. 6 and Table S3 in Smolíková et al. (2022). Calculation of speciation can be done using the physico-chemical data in Table S3 in Smolíková et al. (2022) — ignoring the influence of natural organic matter — with the data from Grenthe et al. (2020) in Thermochimie 11a (Fig. 10b), implemented with Shang and Reiller (2020, 2021a, b) (Fig. 10c), and Prodata 1.5.3.1 (Fig. 10d). Values of dissolved O_2 (Table S3 in Smolíková et al., 2022) assures the predominance of uranium (VI).

As the ratio of concentration of [Mg]/[Ca] — or proportion of activity ratio *x*, see equation (10) — increases from Antwerp (*S* ca. 1 mg L^{-1}) to the sea-ward (*S* ca. 24 mg L^{-1}), it can be seen in Fig. 10b,c,d that the $MgUO_2(CO_3)_3^{2-}$ complex must be implemented in the database — it was not implemented in the calculation in Smolíková et al. (2022) (Fig. 10a) — as it increases with *S* (and concentration of Mg outlined by the value of *x*) for the three other cases (Fig. 10b,c,d). Furthermore, the values of $\varepsilon(Ae_nUO_2(CO_3)_3^{(4-2n)-}, Na^+Cl^-)$ are strongly impacting the speciation results (vide ante), particularly when closing the sea-ward at the highest *S* value. This is closely reminiscent of the analysis of a Canadian aquitard (Reiller and Descostes, 2020; Reiller et al., 2012).

3.1.3. Particular case of temperature in radioactive waste management sites

In the deep underground envisaged laboratories for the management of radioactive waste, the speciation of uranium in solution is under many conditions around the limit between $U(OH)_4$(aq) and $Ca_nUO_2(CO_3)_3^{(4-2n)-}$ (Grivé et al., 2015; Reiller and Descostes, 2020). The differences in pH, E_h (or pe), and activities of Ca^{2+}, Mg^{2+}, HCO_3^-, and Na^+ are driving the proportions of species (Reiller and Descostes, 2020). The activity products can also be usefully employed: pH + pe, $\log_{10}(a(Ae^{2+})/a(H^+)^2)$, $\log_{10}(a(HCO_3^-)\ a(H^+))$, $\log_{10}(a(Na^+)/a(H^+))$, and $\log_{10}(a(Ae^{2+})\ a(HCO_3^-)^2)$ (Lee et al., 2019; Shang et al., 2023).

In Shang and Reiller (2021b), speciation calculations of uranium have been proposed in waters representative of radioactive waste management laboratory sites in Belgium (De Craen et al., 2004) and France (Gaucher et al., 2009) at temperature between 10 and 80 °C. These calculations were done in absence of mineral buffer, and using amorphous UO_2 with no $\Delta_r H°_m$ values selected in the Thermochimie 9b database file used then — taken from Guillaumont et al. (2003) —, which induced the reduction of U(VI) to U(IV), but also of S(VI) to S(-II), and C(IV) to C(-IV). Even if it was specified that the absence of mineralogical buffer could lead to a biased view of the actual situation, a more complete calculation could be proposed to further clarify the situation of the $Ae_nUO_2(CO_3)_3^{(4-2n)-}$ complexes under these conditions.

Table 6
Gibbs energies and enthalpies of reaction, $\log_{10}K°$ and redox potentials calculated from functions of formation in Table 5, unless noted otherwise.

Reaction	$\Delta_r G°_m$ (kJ mol^{-1})	$\Delta_r H°_m$ (kJ mol^{-1})	$\log_{10}K°$	E° (V)
FeS_2(cr) + 9H_2O + CO_2(g) ⇄ $FeCO_3$(cr) + 18H^+ + 2SO_4^{2-} + 14e$^-$	523.287 ± 2.047	568.321 ± 2.068	−91.66 ± 0.36	0.387
FeS_2(cr) + 9H_2O + CO_2(g) ⇄ $FeCO_3$(cr) + 4H^+ + 2SO_4^{2-} + 7H_2(g)				
FeS_2(cr) + 3.5O_2(g) + CO_2(g) + 2H_2O ⇄ $FeCO_3$(cr) + 4H^+ + 2SO_4^{2-}	−1136.693 ± 2.015	−1432.489 ± 2.036	199.11 ± 0.35	–
FeS_2(cr) + 8H_2O + CO_3^{2-} ⇄ $FeCO_3$(cr) + 16H^+ + 2SO_4^{2-} + 14e$^-$	429.674 ± 2.072	564.211 ± 2.072	−75.26 ± 0.36	0.318
FeS_2(cr) + 8H_2O + CO_3^{2-} ⇄ $FeCO_3$(cr) + 2H^+ + 2SO_4^{2-} + 7H_2(g)				
FeS_2(cr) + 3.5O_2(g) + CO_3^{2-} + H_2O ⇄ $FeCO_3$(cr) + 2H^+ + 2SO_4^{2-}	−1240.306 ± 2.047	−1436.599 ± 2.048	217.26 ± 0.36	–
$MgCa(CO_3)_2$(cr) ⇄ Mg^{2+} + Ca^{2+} + 2CO_3^{2-}	−97.757	−35.96[a]	−17.13[a]	
Mg^{2+} + H^+ + CO_3^{2-} ⇄ $MgHCO_3^+$	−64.9	−12.859[b]	11.37[b]	
Mg^{2+} + CO_3^{2-} ⇄ $MgCO_3$(aq)	−17.01	8.804[c]	2.98[c]	
$CaCO_3$(cr) ⇄ Ca^{2+} + CO_3^{2-}	−48.408	−10.62[d]	−8.48[d]	
Ca^{2+} + H^+ + CO_3^{2-} ⇄ $CaHCO_3^+$	−65.243	−23.595[e]	11.43[e]	
Ca^{2+} + CO_3^{2-} ⇄ $CaCO_3$(aq)	−18.38	14.83[e]	3.22[e]	

[a] Robie and Hemingway (1995).
[b] Shock and Koretsky (1995).
[c] Sverjensky et al. (1997), and.
[d] Plummer and Busenberg (1982) from Thermochimie 11a database file.
[e] Thermochimie 11a database file.

The E_h value of the in situ pore-water proposed by Gaucher et al. (2009) — i.e. $E_h = -199$ mV at pH = 7.2 and t = 25 °C — or by De Craen et al. (2004) — i.e. $E_h = -274$ mV at pH = 8.5 and t = 16 °C — can be represented by an equimolar mixture of FeS_2/$FeCO_3$ (pyrite/siderite) — siderite has been found slightly oversaturated in the Mol aquifer (Beaucaire et al., 2000). The thermodynamic functions in Table 5 (Grenthe et al., 2020; Lemire et al., 2013, 2020) can be used to calculate the $\log_{10}K°$ values (Table 6).

A PhreeqC calculation at pH 7.2 and 25 °C using the data from Table 6 gives pe = −2.905 (E_h = −171.9 mV, t = 25 °C). Using the composition in Table 1 from Gaucher et al. (2009).

Concerning Ca and Mg buffering, the use of calcite and dolomite is widespread (Beaucaire et al., 2000). From a thermodynamic point of view (Table 6), calcium is slightly more supersaturated relative to dolomite than to calcite both for Mol — as already evidenced by Beaucaire et al. (2000) using slightly different $\log_{10}K°$ values — and Callovo-Oxfordian formations. Hence, a calculation for Mol using De Craen et al. (2004) gives SI = 0.11 and 0.53 for calcite and dolomite,

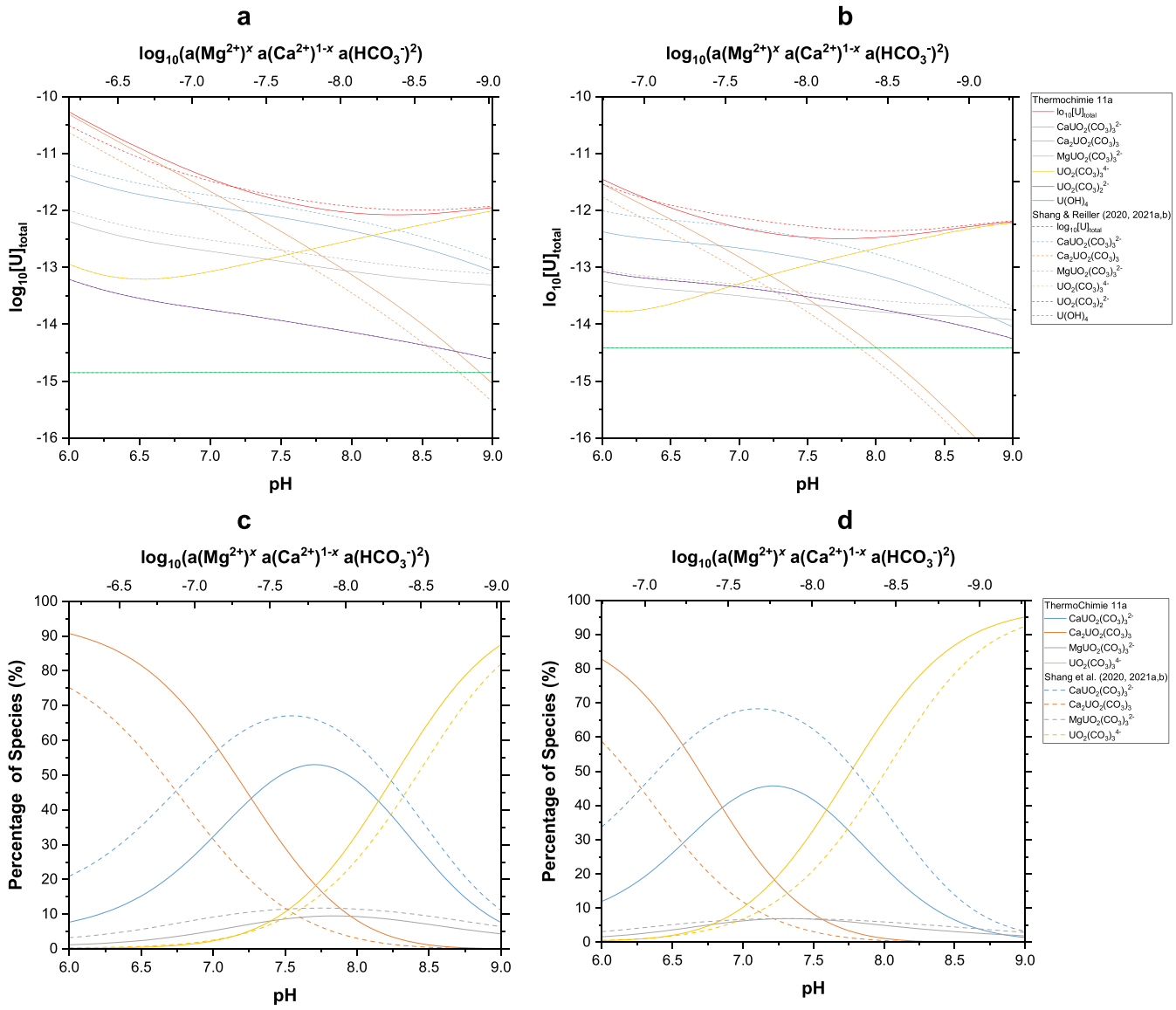

Fig. 11. Solubility of uraninite (a,b) and solution speciation of uranium (c,d) vs. pH — and $\log_{10}(a(Mg^{2+})^x\ a(Ca^{2+})^{1-x}\ a(HCO_3^-)^2)$ — at equilibrium with pyrite, siderite, and dolomite at 25 (a,c) and 50 °C (b,d), from the composition of pore-water from the Mol pore-water (De Craen et al., 2004), using Thermochimie 11a database and thermodynamic functions and SIT parameters for $Ae_nUO_2(CO_3)_3^{(4-2n)-}$ from Shang and Reiller (2020, 2021a, b). Only species with concentration permanently higher than 5% or higher than $U(OH)_4$(aq) are plotted.

respectively; the calculation for Callovo-Oxfordian using Gaucher et al. (2009) gives SI = 0.14 and 0.33 for calcite and dolomite, respectively.

The speciation of uranium vs. temperature was done using two strategies: (i) 6 ≤ pH ≤ 9 speciation was done at 25 and 50 °C at equilibrium with pyrite, siderite, and dolomite; and (ii) the varying temperature allowing pH to equilibrate with pyrite siderite, and dolomite — it can be noted that the increase in temperature from 25 to 50 °C decreases pH from 7.20 (pe = −3.36) to 7.06 (pe = −3.12) for Callovo-Oxfordian water, and from pH = 8.5 (pe = −4.36) to pH = 8.17 (pe = −5.05) for the Mol water composition. Uranium was equilibrated with mineral uraninite (crystalline UO_2) in order to avoid the bias of the absence of $\Delta_rH°_m$ for amorphous UO_2 identified in Shang and Reiller (2021b). Figs. 11 and 12 are showing the solubility and speciation diagrams at varying pH — and $\log_{10}(a(Mg^{2+})^x\ a(Ca^{2+})^{1-x}\ a(HCO_3^-)^2)$ — at 25 °C (Fig. 11a–c and Fig. 12a–c), and 50 °C (Fig. 11b–d and Fig. 12b–d) implementing (dashed lines) or not (plain lines) the thermochemical data and SIT parameters from Shang and Reiller (2020, 2021a, b). As awaited from the ionic strength evolution (Fig. 8) the differences of solubility and speciation between Thermochimie 11a and Shang and Reiller (2020, 2021a, b) are limited, but significant nonetheless. The general comportment of uranium at 25 °C in Callovo-Oxfordian pore-water calculated in previous studies (Shang and Reiller, 2020, 2021a, 2021b), is again evidenced here. At lower pH and higher $\log_{10}(a(Mg^{2+})^x\ a(Ca^{2+})^{1-x}\ a(HCO_3^-)^2)$, the increasing dolomite solubility is favouring the formation of $Ca_nUO_2(CO_3)_3^{(4-2n)-}$ in both cases, but the higher carbonate, or $\log_{10}(a(Mg^{2+})^x\ a(Ca^{2+})^{1-x}\ a(HCO_3^-)^2)$, in Mol is favouring the predominance of $UO_2(CO_3)_3^{4-}$ at high pH at the expenses of $U(OH)_4$(aq), which dominates the speciation under Callovo-Oxfordian conditions. The situation is slightly different at 50 °C as the predominance of $Ca_nUO_2(CO_3)_3^{(4-2n)-}$ is narrowed to lower pH values. In Mol water the situations are comparable — yet slightly shifted to lower pH, or higher $\log_{10}(a(Mg^{2+})^x\ a(Ca^{2+})^{1-x}\ a(HCO_3^-)^2)$. In Callovo-Oxfordian conditions, if $Ca_2UO_2(CO_3)_3$(aq) is still predominant at lower pH or higher $\log_{10}(a(Mg^{2+})^x\ a(Ca^{2+})^{1-x}\ a(HCO_3^-)^2)$ — due to the higher $[Ca]_{total}$ —, as the predominance of $U(OH)_4$(aq) occurs at lower pH or higher $\log_{10}(a(Mg^{2+})^x\ a(Ca^{2+})^{1-x}\ a(HCO_3^-)^2)$ values, $CaUO_2(CO_3)_3^{2-}$ is slightly predominant over a narrow pH or $\log_{10}(a(Mg^{2+})^x\ a(Ca^{2+})^{1-x}\ a(HCO_3^-)^2)$ range. The decreasing $\log_{10}a(Ca^{2+})$ and $\log_{10}(a(Ca^{2+})/a(H^+)^2)$ values

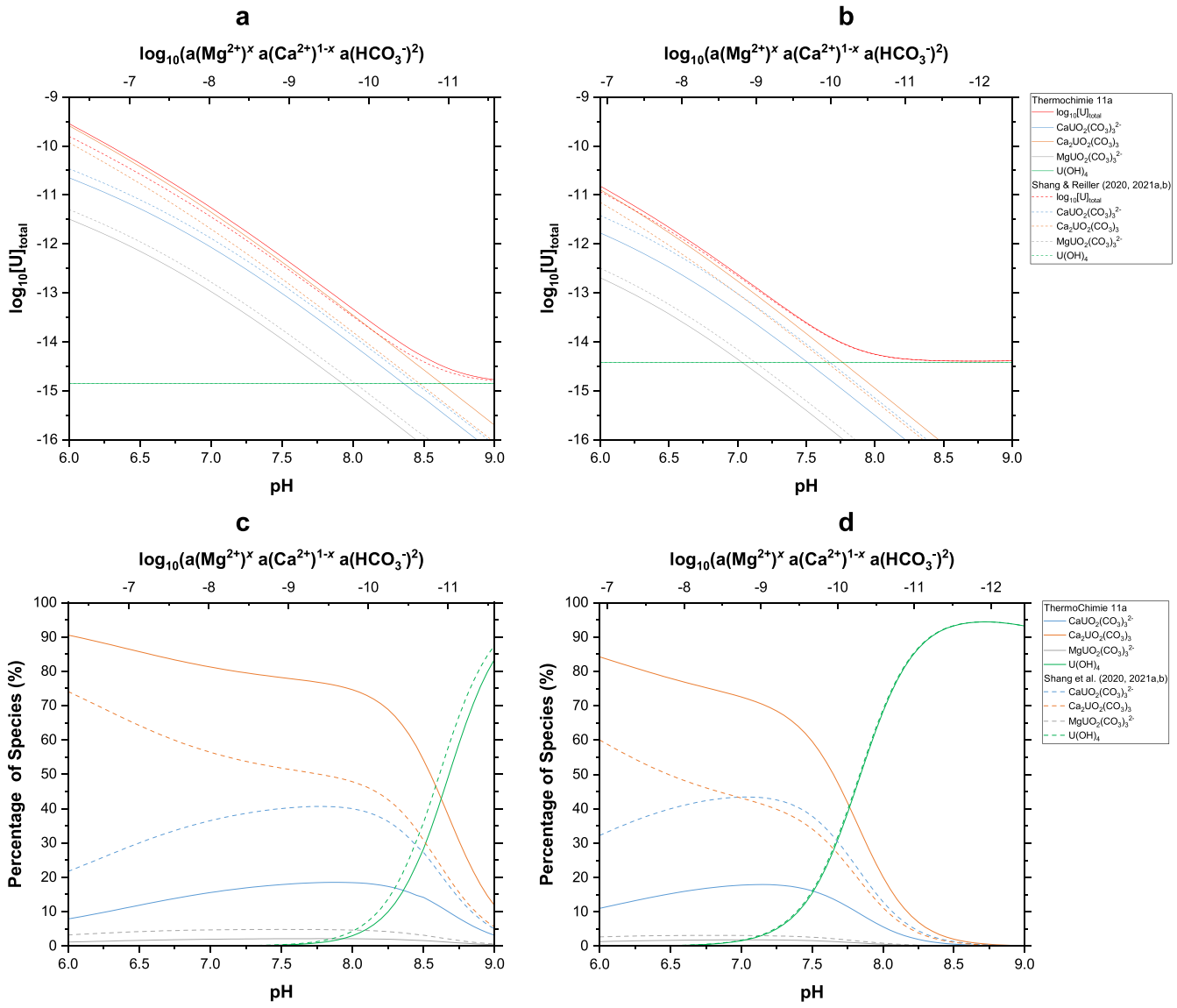

Fig. 12. Solubility of uraninite (a,b) and speciation of dissolved uranium (c,d) vs. pH — and $\log_{10}(a(Mg^{2+})^x\ a(Ca^{2+})^{1-x}\ a(HCO_3^-)^2)$ — at equilibrium with pyrite, siderite, and dolomite at 25 (a,c) and 50 °C (b,d), from the composition of pore-water from the Callovo-Oxfordian formation (Gaucher et al., 2009), using Thermochimie 11a database (plain) and thermodynamic functions and SIT parameters for $Ae_nUO_2(CO_3)_3^{(4-2n)-}$ from Shang and Reiller (2020, 2021a, b) (dashed). Only species higher than 5% are plotted.

compared to 25 °C is monitoring and explaining the lower solubility increase of uraninite and lower predominance of $Ca_2UO_2(CO_3)_3(aq)$.

Fig. 13 is showing the variation of speciation of dissolved uranium from uraninite at equilibrium with pyrite, siderite, and dolomite, at varying temperature, and the accompanying $\log_{10}(a(Mg^{2+})^x\ a(Ca^{2+})^{1-x}\ a(HCO_3^-)^2)$ decrease for Mol (Fig. 13a) and Callovo-Oxfordian (Fig. 13b). It shows that with decreasing pH — and accompanying decrease in $\log_{10}(a(Ca^{2+})/a(H^+)^2)$ values —, the predominance of $Ca_2UO_2(CO_3)_3(aq)$ is lowered to the benefit of $CaUO_2(CO_3)_3^{2-}$, leaving only a small amount of $U(OH)_4(aq)$. These calculations mitigate the calculations in Shang and Reiller (2021b), and are giving a more complete vision of the importance of these complexes.

3.2. Plutonium

The formal oxidation potentials of the free ions of plutonium calculated from the Gibbs energies in Grenthe et al. (2020) are reported in Fig. 14 — it can be noted that extensive hydrolysis of Pu(IV) induces that Pu^{4+} represent ca. 72% at pH = 0 in $HClO_4$.

Recently, Jo et al. (2020) studied the formation of $MgPuO_2(CO_3)_3^{2-}$ and $CaPuO_2(CO_3)_3^{2-}$ complexes; no formation of $Ae_2PuO_2(CO_3)_3(aq)$ was evidenced. The formation of the $AePuO_2(CO_3)_3^{2-}$ complexes are thought to principally impact the equilibrium between Pu(V) and Pu(VI) in oxic carbonated media, viz. pe > 8, and 8 < pH < 9.25 (Jo et al., 2022). Nevertheless, further estimation or determination of the $\log_{10}\beta^\circ$ and ε values are still desirable for the reasons seen for uranium (vide supra).

3.2.1. Experiment vs. LFER estimation

The formation of the $Ae_nPuO_2(CO_3)_3^{(4-2n)-}$ complexes could have been estimated from the LFER in Fig. 1 between inorganic ligand $\log_{10}\beta^\circ$ using thermochemical data selection for U, Np, and Pu (Grenthe et al., 1992, 2020; Guillaumont et al., 2003; Lemire et al., 2001).

The regression uncertainty calculated using the parameters in Table 3 cannot be better that 1.6 logarithmic unit for estimated $\log_{10}\beta^\circ_{Pu}$ values. As the $\log_{10}\beta^\circ(Ae_nAnO_2(CO_3)_3^{(4-2n)-})$ are deeply dependent on the $\log_{10}\beta^\circ(AnO_2(CO_3)_3^{4-})$ values that are different for U, Np, and Pu (Table 1), the estimation via the LFERs will be done using the successive

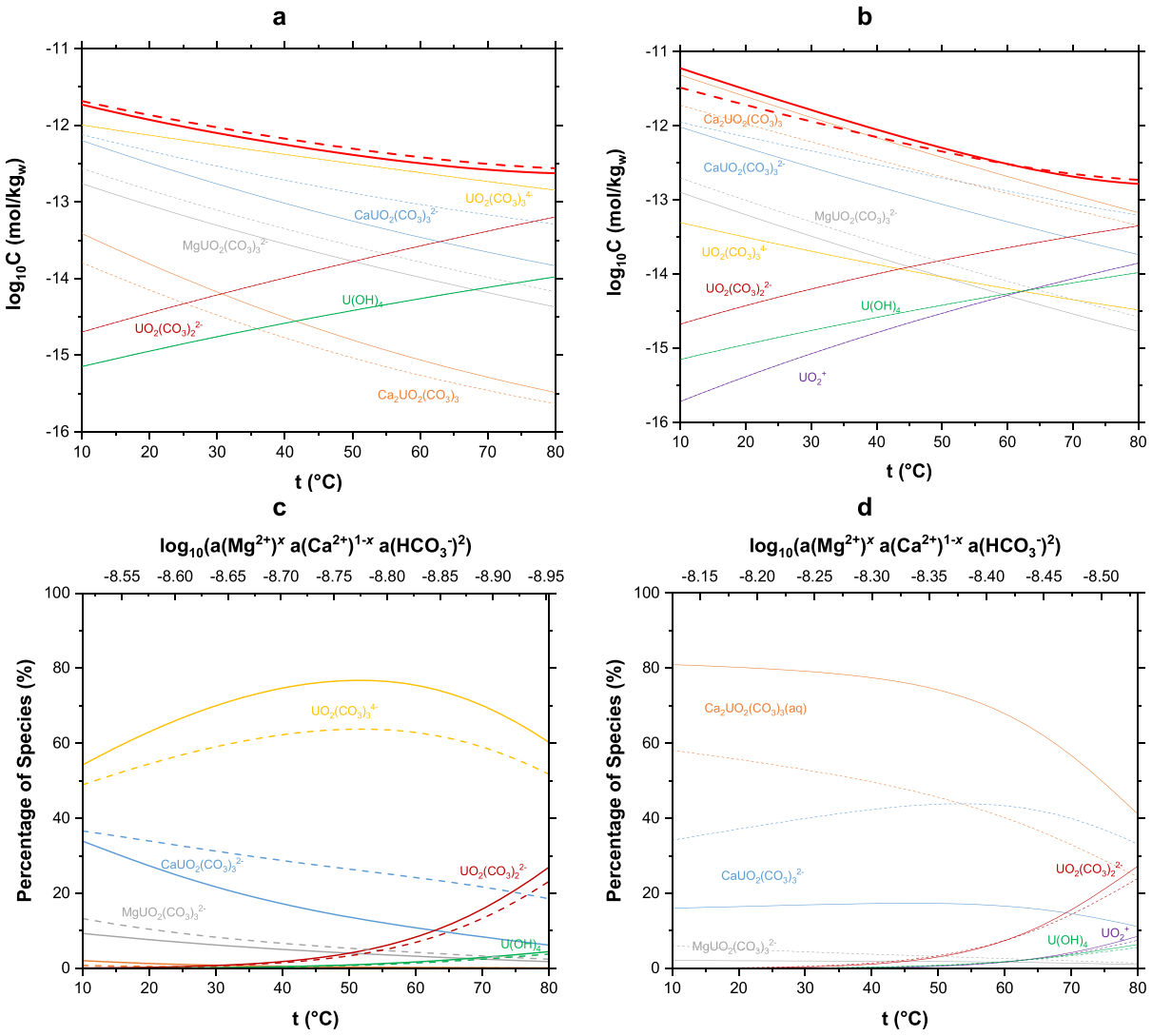

Fig. 13. Solubility of uraninite (a,b) and speciation of dissolved uranium (c,d) vs. temperature — and $\log_{10}(a(Mg^{2+})^x\ a(Ca^{2+})^{1-x}\ a(HCO_3^-)^2)$ — calculated at equilibrium with pyrite, siderite, and dolomite allowing pH to equilibrate, from the initial composition of pore-water from the Mol (De Craen et al., 2004) (a,c) and Callovo-Oxfordian (Gaucher et al., 2009) (b,d) formations, using Thermochimie 11a database (plain) and $\log_{10}\beta^\circ(Ae_nUO_2(CO_3)_3^{(4-2n)-})$ and $\varepsilon(Ae_nUO_2(CO_3)_3^{(4-2n)-}, Na^+Cl^-)$ from Shang and Reiller (2020, 2021b) (dashed).

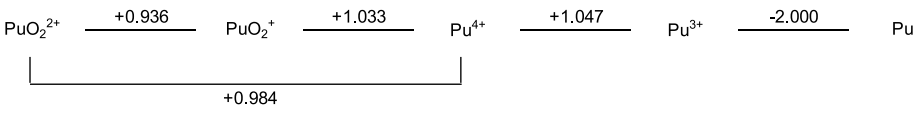

Fig. 14. The formal oxidation potential (Volt) diagram of plutonium in acidic aqueous solutions (Grenthe et al., 2020).

experimental constants $\log_{10}K^\circ$.

The estimated $\log_{10}K^\circ$ values for eventual $MgPuO_2(CO_3)_3^{2-}$, $CaPuO_2(CO_3)_3^{2-}$, and $Ca_2PuO_2(CO_3)_3(aq)$ are plotted in Fig. 1, and reported in Table 4, together with the values determined experimentally by Jo et al. (2020). There is a very good agreement between the experimental $\log_{10}K^\circ(MgPuO_2(CO_3)_3^{2-}) = 4.29 \pm 0.18$ and the estimated values for the stepwise reaction, either using the experimental data of $MgUO_2(CO_3)_3^{2-}$ from Shang and Reiller (2021a) ($\log_{10}K^\circ = 4.5 \pm 1.6$) or from the selected value in Grenthe et al. (2020) or determined in Fig. 4 ($\log_{10}K^\circ = 4.4 \pm 1.6$). The $Mg_2PuO_2(CO_3)_3(aq)$ species have not been detected by Jo et al. (2020) and should be regarded with caution.

There is a fairly good agreement between the experimental $\log_{10}K^\circ(CaPuO_2(CO_3)_3^{2-}) = 6.05 \pm 0.50$ and the estimated values for the stepwise reaction, either using the experimental data of $CaUO_2(CO_3)_3^{2-}$ from Shang and Reiller (2020) ($\log_{10}K^\circ = 5.3 \pm 1.6$) or from the selected value in Grenthe et al. (2020) ($\log_{10}K^\circ = 5.1 \pm 1.6$) or determined in Fig. 4 ($\log_{10}K^\circ = 5.2 \pm 1.6$). Because of the value of the stepwise reaction constant between $CaUO_2(CO_3)_3^{2-}$ and $Ca_2UO_2(CO_3)_3(aq)$, the $Ca_2PuO_2(CO_3)_3(aq)$ complex may have been difficult to evidence under the conditions used by Jo et al. (2020). Applying $\log_{10}K^\circ(CaPuO_2(CO_3)_3^{2-}) = 6.05$ from Jo et al. (2020) and $\log_{10}K^\circ(Ca_2PuO_2(CO_3)_3(aq)) = 3.2$ (Table 4), then $Ca_2PuO_2(CO_3)_3(aq)$ would only account for ca. 6% at the highest calcium concentration used (Fig. S4 of the SI).

The cumulative constants $\log_{10}\beta^\circ$ for the $MgPuO_2(CO_3)_3^{2-}$ and $CaPuO_2(CO_3)_3^{2-}$ complexes can be estimated using $\log_{10}\beta^\circ(PuO_2(CO_3)_3^{4-})$ in Table 1. In both cases the estimated $\log_{10}\beta^\circ(AePuO_2(CO_3)_3^{2-})$ values are in agreement with the one obtained from the determination of Jo

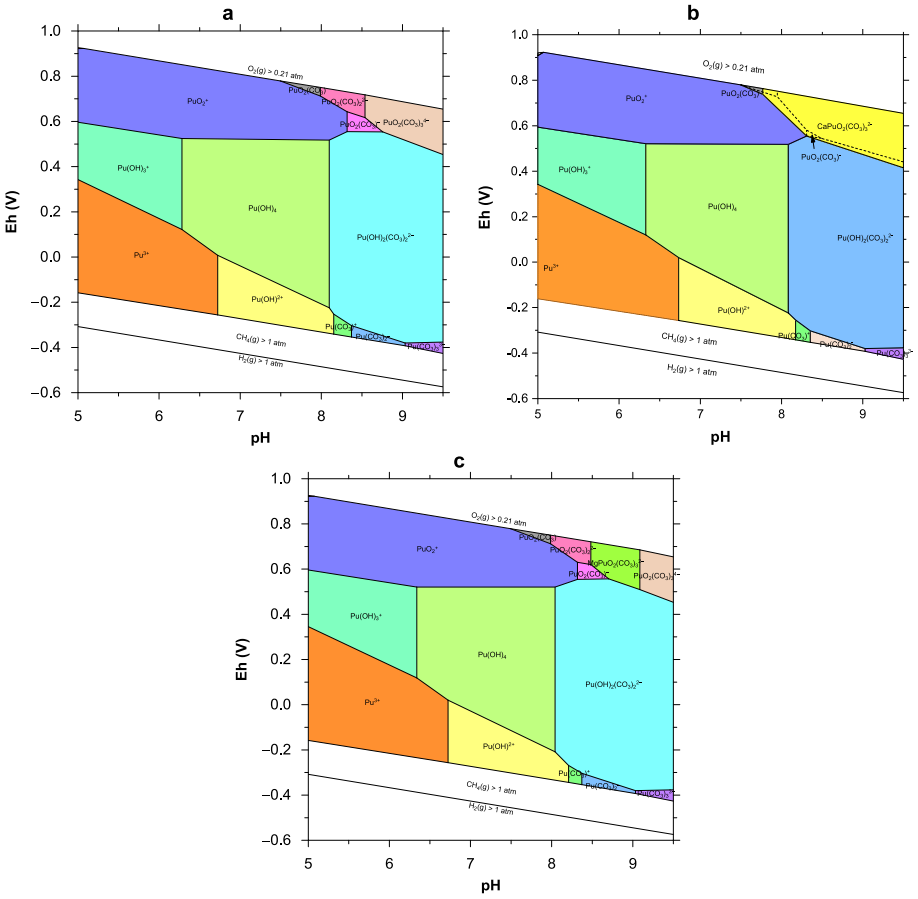

Fig. 15. Pourbaix diagrams (Kinniburgh and Cooper, 2011) of [Pu] = 0.1 nmol kg_w^{-1} (a,b,c), I_m = 0.1 mol kg^{-1} NaCl, and $P(CO_2) = 10^{-3.5}$ atm (Grenthe et al., 2020); not considering (a) and considering the $CaPuO_2(CO_3)_3^{2-}$ (b) or $MgPuO_2(CO_3)_3^{2-}$ (c) complexes from Jo et al. (2020) (plain line) or from LFER (dashed line); [Ae] = 5 mmol kg_w^{-1} (Ae is Ca (b) or Mg (c)), and considering $\varepsilon(AePuO_2(CO_3)_3^{2-},Na^+Cl^-) = \varepsilon(AeUO_2(CO_3)_3^{2-},Na^+Cl^-)$ from Shang and Reiller (2020) (b) and Shang and Reiller (2021a) (c); no precipitation required.

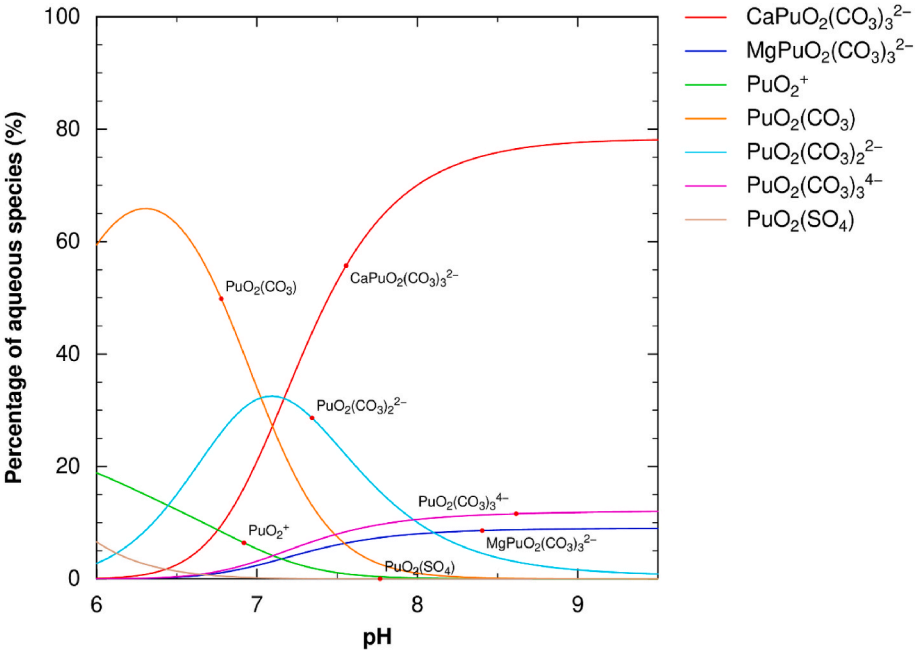

Fig. 16. Speciation of [Pu] = 0.1 nmol kg_w^{-1} in standard seawater (Millero et al., 2008), at $P(O_2) = 0.2095$ atm, using Jo et al. (2020) constants for $MgPuO_2(CO_3)_3^{2-}$ and $CaPuO_2(CO_3)_3^{2-}$, and ε values from Shang and Reiller (2020, 2021a) in analogy.

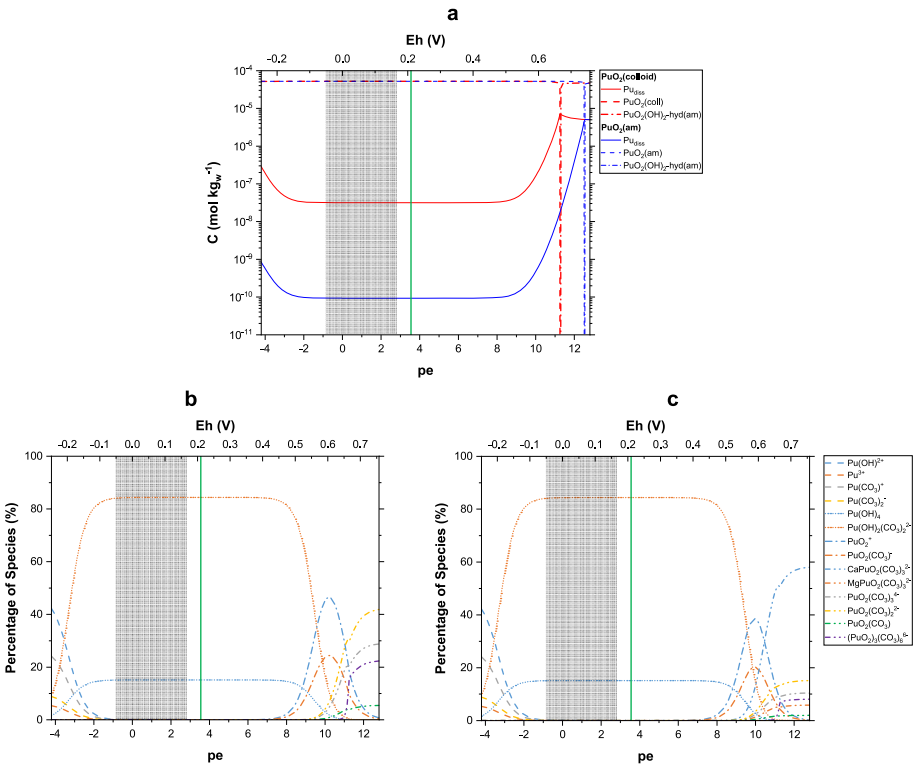

Fig. 17. Solubility (a) and speciation in solution (b,c) of Pu from Dumas et al. (2018) including precipitation of PuO_2:2H_2O(am) (a) or PuO_2(coll) (a,b,c), and $PuO_2(OH)_2$:H_2O(cr) using Thermochimie 11a (b), and implemented with the $AePuO_2(CO_3)_3^{2-}$ complex (Jo et al., 2020) and $\varepsilon(AeUO_2(CO_3)_3^{(4-2n)-},Na^+Cl^-)$ (Shang and Reiller, 2020, 2021a) in analogy, at pH 7.88 and varying pe: green thick plain line and shaded red domain indicate the measured E_h value from Dumas et al. (2018) and Meyer et al. (2014), respectively. (For interpretation of the references to colour in this figure legend, the reader is referred to the Web version of this article.)

et al. (2020). The estimation of the potential Sr^{2+} and Ba^{2+} complexes for PuO_2^{2+}, using the U-selected values by Grenthe et al. (2020) are also given in Table 4 for scoping calculation.

It can also be noted that the $\log_{10}K^\circ$ values obtained by Jo et al. (2020) after extrapolation to infinite dilution using Davies (1962) equation are no different than the ones that could be obtained using the $\varepsilon(AeUO_2(CO_3)_3^{(4-2n)-},Na^+Cl^-)$ values in Shang and Reiller (2020, 2021a) in analogy (Table 2), i.e. $\log_{10}K^\circ(CaUO_2(CO_3)_3^{2-},Na^+Cl^-) = 6.05 \pm 0.50$ and $\log_{10}K^\circ(MgUO_2(CO_3)_3^{2-},Na^+Cl^-) = 4.32 \pm 0.18$.

The values of Mg and Ca complexes from Jo et al. (2020) and from the LFER — only estimation from Shang and Reiller (2020, 2021a) — are used to draw the Pourbaix diagrams at $I_m = 0.1$ mol kg_w^{-1} NaCl, and $P(CO_2) = 10^{-3.5}$ atm (Fig. 15a), [Ca] = 5 mmol kg_w^{-1} (Fig. 15b), and [Mg] = 5 mmol kg_w^{-1} (Fig. 15c) using the Thermochimie 11a database — one can note the importance of $Pu(OH)_2(CO_3)_2^{2-}$, which was not selected in Grenthe et al. (2020). The SIT parameters from Shang and Reiller (2020, 2021a) are used in analogy. It can be seen that the $MgPuO_2(CO_3)_3^{2-}$ and $CaPuO_2(CO_3)_3^{2-}$ complexes are not awaited to have any influence on the chemistry of Pu under the conditions of the underground research laboratories in Belgium (De Craen et al., 2004; Honty et al., 2022; Wang et al., 2023), France (Gaucher et al., 2009; Vinsot et al., 2008), Sweden (Emrén et al., 1999), or Switzerland (Courdouan Merz, 2008; Montoya et al., 2021; Thury and Bossart, 1999), where equivalent $P(CO_2)$ is ca. 10^{-2} atm. The Pu speciation calculated for the Callovo-Oxfordian water (Gaucher et al., 2009) at varying pH and constant $P(O_2) = 10^{-65.7}$ atm corresponding to the pe is shown in Fig. S6a of the SI suggesting a Pu (III)/Pu(IV) mixture. The speciation at constant pH = 7.1, and varying pe from the site value to atmospheric O_2(g), not accounting (Fig. S6b of the SI) and accounting (Fig. S6c of the SI) for the $AePuO_2(CO_3)_3^{2-}$ complexes from Jo et al. (2020). The $CaPuO_2(CO_3)_3^{2-}$ complex nevertheless extends significantly the Pu(VI) domain in oxidized mildly alkaline media, particularly in carbonated calcium and magnesium media, more at the expenses of Pu(V) than of Pu(IV).

The question of the potential importance of these complexes in seawater should then be addressed directly.

3.2.2. *Application to standard seawater*

The most striking parameter affecting the chemistry of Pu in seawater is the redox potential. The E_h varies with depth (McManus et al., 2005) with the dissolved oxygen concentration. However, measurements did not seem to follow the O_2/H_2O equilibrium but other oxygen equilibria (Meyer et al., 2014). Particularly, the equilibria including superoxide radical $O_2^{\cdot-}/H_2O_2$ and $O_2/O_2^{\cdot-}$ have been proposed to control the redox with depth.

In sea and ocean waters, speciation of plutonium seem to be driven by Pu(VI + V)/Pu(IV), as suggested by Fig. 15: Nelson and Lovett (1978) seemed to favour Pu(VI)/Pu(IV). Aston (1980) estimated that dissolved Pu in seawater should likely be under the form of Pu(VI) species with Pu (IV) as colloidal form. The complex $PuO_2OHCO_3^-$ proposed then was afterwards disregarded in the first NEA-OECD commissioned review for Pu (Lemire et al., 2001).

McManus et al. (2005) proposed dissolved oxygen concentrations in deep Pacific Ocean samples that would suggest the predominance of Pu (VI) in solution, even if redox in sea and ocean waters is more complicated (Meyer et al., 2014).

A speciation calculation using the data from Jo et al. (2020), and ε values from Shang and Reiller (2020, 2021a) in analogy, and the seawater composition from Millero et al. (2008) is drawn in Fig. 16 at $P(O_2) = 0.2095$ atm and varying pH — the carbonate concentration is not equilibrated either with atmospheric CO_2 (SI = −3.29) or alkaline earth carbonate phases such as calcite ($CaCO_3$, SI = 0.35), magnesite ($MgCO_3$, SI = 0.81), nesquehonite ($MgCO_3$:3H_2O, SI = −2.15), or dolomite ($MgCa(CO_3)_2$, SI = 1.77, or $Mg_{0.5}Ca_{0.5}CO_3$, SI = 0.89). At pH = 8.1 of the standard seawater proposed by Millero et al. (2008), it can be seen that $CaPuO_2(CO_3)_3^{2-}$ is calculated to be ca. 72% and $MgPuO_2(CO_3)_3^{2-}$ ca. 8% and are the major and fourth major species, respectively — $PuO_2(CO_3)_2^{2-}$

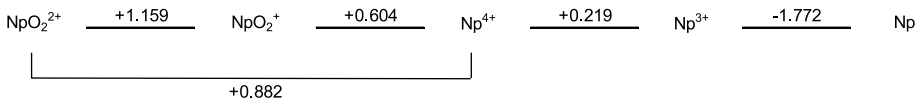

Fig. 18. The formal oxidation potential (Volt) diagram of neptunium in acidic aqueous solutions (Grenthe et al., 2020).

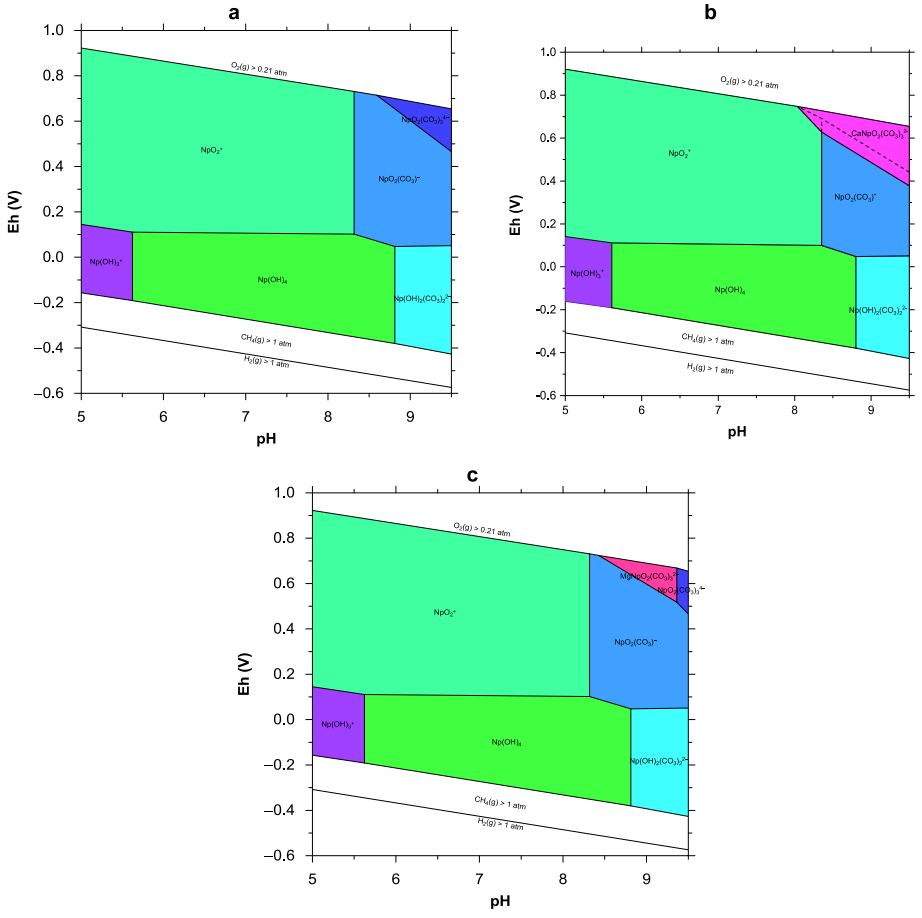

Fig. 19. Pourbaix diagram (Kinniburgh and Cooper, 2011) of [Np] = 0.1 nmol kg^{-1}, I_m = 0.1 mol kg_w^{-1} NaCl, and $P(CO_2) = 10^{-3.5}$ atm (Grenthe et al., 2020); not considering (a) and considering the $Ae_nPuO_2(CO_3)_3^{(4-2n)-}$ complexes in Table 4 (b,c); [Ae] = 5 mmol kg_w^{-1} — Ae = Ca (b), Ae = Mg (c) —, $\log_{10}\beta^\circ(Ca_nNpO_2(CO_3)_3^{(4-2n)-})$ estimated from LFER (Table 4) from Shang and Reiller (2020) (b, dashed lines) and Jo et al. (2020) (b, plain lines) and considering $\varepsilon(AeNpO_2(CO_3)_3^{2-},Na^+Cl^-) = \varepsilon(AeUO_2(CO_3)_3^{2-},Na^+Cl^-)$ from Shang and Reiller (2020) (b) and Shang and Reiller (2021a) (c); no precipitation required.

ca. 11%, and $PuO_2(CO_3)_3^{4-}$ ca. 8%. It is then evident that the $\log_{10}K^\circ$ values from Jo et al. (2020) need to be confirmed further and ε values determined instead of being estimated by analogy.

These theoretical calculations could be compared to the laboratory experiments from Dumas et al. (2018) where the precipitation of colloidal Pu(IV) was observed after an addition of 50 μmol_{Pu} kg_w^{-1} in a natural seawater sample. The authors measured E_h = 210 mV at pH = 7.8 (8) (pe = 3.54 at 25 °C), which does allow anticipating any influence of $CaPuO_2(CO_3)_3^{2-}$ — cf. Figs. 15b and 17, and Fig. S6 of the SI. This also indicates that the redox potential is not controlled by dissolved oxygen — E_h = 210 mV/NHE at 25 °C would correspond to $P(O_2) = 10^{-37.4}$ atm, or as low as 1.6 10^{-36} mg kg_w^{-1} O_2 — but by another redox couple. This total concentration of Pu would allow the formation of either phases contained in Thermochimie 11a database file: amorphous PuO_2:$2H_2O$ (am) or colloidal PuO_2(coll) (taken from Neck et al., 2007), up to the formation of $PuO_2(OH)_2$:H_2O(am). At pH 7.88, for PuO_2(coll), pe = 11.23, E_h = 0.665 V, 8.9 10^{-6} mg L^{-1} O_2 (Fig. 17), and for PuO_2:$2H_2O$ (am), pe = 12.48, E_h = 738 mV, 0.85 mg kg_w^{-1} O_2 (Fig. S7 of the SI). It can be noted that $Pu(OH)_2(CO_3)_3^{2-}$ from Rai et al. (1999b), which was not selected in Grenthe et al. (2020), strongly dominates the Pu(IV) speciation at the measured E_h value.

Meyer et al. (2014) measured E_h values in the Gotland Deep (Baltic Sea) from −55 to 167 mV at temperature varying from 3 to 8 °C, i.e. pe from −0.99 to 2.99, which would correspond to Pu(IV) predominance.

3.3. Neptunium

The formal oxidation potentials of the free ions of neptunium calculated from the Gibbs energies in Grenthe et al. (2020) are reported in Fig. 18 it can be noted that extensive hydrolysis of Np(IV) induces that Np^{4+} represent ca. 48% at pH = 0 in $HClO_4$.

3.3.1. Estimation by LFER

Up to now, no determination of the formation of $Ae_nNpO_2(CO_3)_3^{(4-2n)-}$ has been reported. From the general agreement between estimated and measured $\log_{10}\beta^\circ(AePuO_2(CO_3)_3^{2-})$ values, a comparable exercise can be proposed for Np. The LFER uncertainty for estimated $\log_{10}\beta^\circ_{Np}$ values cannot be better than 1.1 and 0.7 logarithmic unit from $\log_{10}\beta^\circ_U$ and $\log_{10}\beta^\circ_{Pu}$, respectively. The estimated $\log_{10}K^\circ$ values for eventual $MgNpO_2(CO_3)_3^{2-}$, $CaNpO_2(CO_3)_3^{2-}$, and

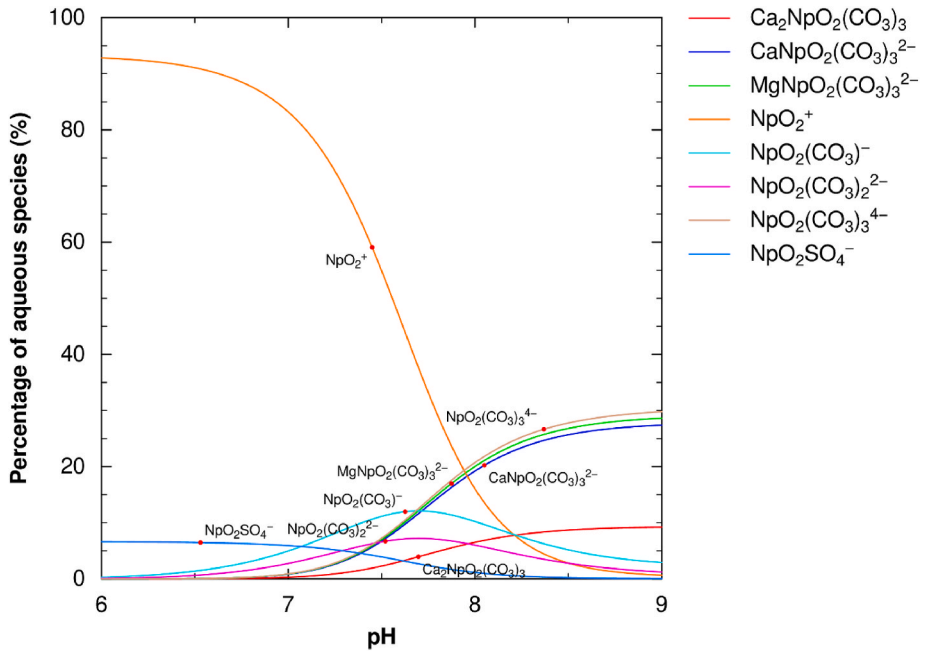

Fig. 20. Speciation of [Np] = 0.1 nmol kg_w^{-1} in standard seawater (Millero et al., 2008), at $P(O_2) = 0.2095$ atm, using $\log_{10}\beta^\circ(Ae_nNpO_2(CO_3)_3^{(4-2n)-})$ in Table 4, and ε values from Shang and Reiller (2020, 2021a) in analogy.

$Ca_2NpO_2(CO_3)_3(aq)$ are plotted in Fig. 2, and reported in Table 4. Here again, $Ca_2NpO_2(CO_3)_3(aq)$ has to be regarded with caution as long as the hypothesis on plutonium is not verified (vide ante). The values for $MgNpO_2(CO_3)_3^{2-}$, estimated either from $\log_{10}\beta^\circ_U$ and $\log_{10}\beta^\circ_{Pu}$ LFERs are in excellent agreement whatever the origin of the constants and LFER used, i.e. $\log_{10}K^\circ = 4.5 \pm 1.1$ from Shang and Reiller (2021a) (Table 4, Fig. 2), and $\log_{10}K^\circ = 4.3 \pm 1.1$ from Grenthe et al. (2020) (Table 4) using $\log_{10}\beta^\circ_U = f(\log_{10}\beta^\circ_{Np})$, and $\log_{10}K^\circ = 4.5 \pm 0.7$ from Jo et al. (2020) using $\log_{10}\beta^\circ_{Pu} = f(\log_{10}\beta^\circ_{Np})$ (Table 4, Fig. 3).

In the case of $CaNpO_2(CO_3)_3^{2-}$, the agreement is fair considering the uncertainties. Using the $\log_{10}\beta^\circ_U = f(\log_{10}\beta^\circ_{Np})$ LFER, a $\log_{10}K^\circ(CaNpO_2(CO_3)_3^{2-}) = 5.3 \pm 1.1$ from Shang and Reiller (2020) (Table 4, Fig. 2), and $\log_{10}K^\circ(CaNpO_2(CO_3)_3^{2-}) = 5.1 \pm 1.1$ from Grenthe et al. (2020), whereas $\log_{10}K^\circ(CaNpO_2(CO_3)_3^{2-}) = 6.3 \pm 0.7$ is obtained from Jo et al. (2020) using $\log_{10}\beta^\circ_{Pu} = f(\log_{10}\beta^\circ_{Np})$ (Table 4, Fig. 3). The value for $Ca_2NpO_2(CO_3)_3(aq)$ can only be estimated using $\log_{10}\beta^\circ_U = f(\log_{10}\beta^\circ_{Np})$ LFER: a $\log_{10}K^\circ(Ca_2NpO_2(CO_3)_3(aq)) = 3.2 \pm 1.1$ from Shang and Reiller (2020) (Table 4, Fig. 2), and $\log_{10}K^\circ(Ca_2NpO_2(CO_3)_3(aq)) = 3.7 \pm 1.1$ from Grenthe et al. (2020). Here again, as Jo et al. (2020) did not evidenced the formation of $Ca_2PuO_2(CO_3)_3(aq)$, this latter value should regarded with caution. The cumulative constants in Table 4 are calculated accounted for the formation of $NpO_2(CO_3)_3^{4-}$ (Table 1).

The values of Mg and Ca complexes in Table 4 are used to draw the Pourbaix diagrams at $I_m = 0.1$ mol kg_w^{-1} NaCl, and $P(CO_2) = 10^{-3.5}$ atm (Fig. 19a), [Ca] = 5 mmol kg_w^{-1} — Fig. 19b using Shang and Reiller (2020) and Jo et al. (2020) —, and [Mg] = 5 mmol kg_w^{-1} — Fig. 19c using Shang and Reiller (2021a) — implemented in the input file using the Thermochimie 11a database — one can note that the selection of Np $(OH)_2(CO_3)_2^{2-}$ from Rai et al. (1999a) strongly impacts the speciation of Np(IV). The SIT parameters from Shang and Reiller (2020, 2021a) are used in analogy. As in the case of Pu, It can be seen that the $Ae_nNpO_2(CO_3)_3^{(4-2n)-}$ complexes are not awaited to have any influence on the chemistry of Np under the conditions of the underground research laboratories in Belgium, France, Sweden, or Switzerland for the same reasons explained beforehand. The $Ca_nNpO_2(CO_3)_3^{(4-2n)-}$ complexes nevertheless extend significantly the Np(VI) domain in oxidized alkaline media — particularly in carbonated calcium and magnesium media —, more at the expenses of NpO_2^+ than of $NpO_2CO_3^-$. The question of the potential importance of these complexes in shallow seawater should also then be addressed.

3.3.2. *Application to standard seawater (Millero et al., 2008)*

The calculated speciation of Np in standard seawater from Millero et al. (2008) in Fig. 20 using data in Table 4, and $\varepsilon(Ae_nUO_2(CO_3)_3^{(4-2n)-}, Na^+Cl^-)$ from Shang and Reiller (2020, 2021a) in analogy suggests that the sum of $Ae_nNpO_2(CO_3)_3^{(4-2n)-}$ could be major in seawater. It seems then desirable to determine both $\log_{10}\beta^\circ(Ae_nNpO_2(CO_3)_3^{(4-2n)-})$ and $\varepsilon(Ae_nNpO_2(CO_3)_3^{(4-2n)-}, Na^+Cl^-)$ values.

4. Conclusion

This study stresses the need to accurately determine the thermochemical constants ($\log_{10}K^\circ$ and $\log_{10}\beta^\circ$) and functions ($\Delta_fG^\circ_m$, $\Delta_fH^\circ_m$, and $S_f^\circ{}_m$), of the $Ae_nAnO_2(CO_3)_3^{(4-2n)-}$ complexes, as well as the specific ion-interaction coefficients ε in relevant ionic media, i.e. NaCl or $NaNO_3$, of the nuclear fuel cycle. The comparisons of calculations using different thermochemical databases showed that implementation of these data are needed for a trustworthy evaluation of the impact of $Ae_nAnO_2(CO_3)_3^{(4-2n)-}$ in slightly alkaline and carbonated media.

With the use of recent data, this study has ascertained the predominance domains of the $Ae_nUO_2(CO_3)_3^{(4-2n)-}$ complexes in terms pH, activities of HCO_3^-, Ca^{2+} and Mg^{2+}, redox potentials (pe, E_h, or dissolved O_2), salinity, and temperature. Linear free energy relationships, based on widely accepted thermochemical data, have been used to estimate the potential predominance of $Ae_nAnO_2(CO_3)_3^{(4-2n)-}$ for Pu and Np. The estimated value for $CaPuO_2(CO_3)_3^{2-}$ is in fair agreement with a recent experimental determination, which allows better defining the predominance of the complex at the expenses of Pu(V) and slightly to Pu(IV). In the case of neptunium, where no experimental evidence has been published at the time of submission, the estimated constant also allows estimating the potential predominance of $AeNpO_2(CO_3)_3^{2-}$ at the expense of Np(V) (NpO_2^+ and $NpO_2(CO_3)^-$).

Hence, the determination of the thermochemical constants and functions, and ε values of $Ae_nPuO_2(CO_3)_3^{(4-2n)-}$ and $Ae_nNpO_2(CO_3)_3^{(4-2n)-}$ in NaCl (at least) are needed for a better evaluation of their predominance in oxidizing to slightly reducing media.

CRediT authorship contribution statement

Pascal E. Reiller: Conceptualization, Data curation, Formal analysis, Investigation, Methodology, Visualization.

Declaration of competing interest

The authors declare the following financial interests/personal relationships which may be considered as potential competing interests: Pascal Reiller reports financial support was provided by National Agency for Radioactive Waste and Enriched Fissile Materials.

Data availability

Data will be made available on request.

Acknowledgement

ONDRAF-NIRAS is acknowledged for its support through contract (DEN4857-CCHO 2018–0456/00/00).

Appendix A. Supplementary data

Supplementary data to this article can be found online at https://doi.org/10.1016/j.chemosphere.2023.141049.

References

Allard, B., Kipatsi, H., Liljenzin, J.O., 1980. Expected species of uranium, neptunium and plutonium in neutral aqueous solutions. J. Inorg. Nucl. Chem. 42, 1015–1027. https://doi.org/10.1016/0022-1902(80)80394-0.

Amayri, S., 2002. Synthese, Charakterisierung und Löslichkeit von Erdalkaliuranylcarbonaten $M_2[UO_2(CO_3)_3]$. Technischen Universität Dresden, Dreden, Germany, p. 182 xH2O; M: Mg, Ca, Sr, Ba. PhD Thesis. http://www.qucosa.de/fileadmin/data/qucosa/documents/2931/5093.pdf.

Aston, S.R., 1980. Evaluation of the chemical forms of plutonium in seawater. Mar. Chem. 8, 319–325. https://doi.org/10.1016/0304-4203(80)90020-1.

Aupiais, J., Christin, C., Levier, M., 2023. Aquatic chemistry of pentavalent plutonium: determination of the first hydrolysis constant. Inorg. Chem. 62, 4533–4539. https://doi.org/10.1021/acs.inorgchem.2c04398.

Beaucaire, C., Pitsch, H., Toulhoat, P., Motellier, S., Louvat, D., 2000. Regional fluid characterisation and modelling of water-rock equilibria in the Boom clay formation and in the Rupelian aquifer at Mol, Belgium. Appl. Geochem. 15, 667–686. https://doi.org/10.1016/S0883-2927(99)00067-0.

Bernhard, G., Geipel, G., Brendler, V., Nitsche, H., 1996. Speciation of uranium in seepage waters of a mine tailing pile studied by time-resolved laser-induced fluorescence spectroscopy (TRLFS). Radiochim. Acta 74, 87–91. https://doi.org/10.1524/ract.1996.74.special-issue.87.

Bernhard, G., Geipel, G., Brendler, V., Nitsche, H., 1998. Uranium speciation in waters of different uranium mining areas. J. Alloys Compd. 271, 201–205. https://doi.org/10.1016/S0925-8388(98)00054-1.

Bernhard, G., Geipel, G., Reich, T., Brendler, V., Amayri, S., Nitsche, H., 2001. Uranyl(VI) carbonate complex formation: validation of the $Ca_2UO_2(CO_3)_3$(aq.) species. Radiochim. Acta 89, 511–518. https://doi.org/10.1524/ract.2001.89.8.511.

Brackett, E.B., Brackett, T.E., Sass, R.L., 1963. Crystal structures of barium chloride, barium bromide, and barium iodide. J. Phys. Chem. 67, 2132–2135. https://doi.org/10.1021/J100804a038.

Brooks, S.C., Fredrickson, J.K., Carroll, S.L., Kennedy, D.W., Zachara, J.M., Plymale, A.E., Kelly, S.D., Kemner, K.M., Fendorf, S., 2003. Inhihition of bacterial U(VI) reduction by calcium. Environ. Sci. Technol. 37, 1850–1858. https://doi.org/10.1021/es0210042.

Brown, P.L., Ekberg, C., 2016. Hydrolysis of Metal Ions. Wiley-VCH Verlag GmbH & Co., Weinheim, Germany https://doi.org/10.1002/9783527656189.

Carvajal, D.A., Katsenovich, Y.P., Lagos, L.E., 2012. The effects of aqueous bicarbonate and calcium ions on uranium biosorption by *Arthrobacter* G975 strain. Chem. Geol. 330, 51–59. https://doi.org/10.1016/j.chemgeo.2012.08.018.

Chase, M.W., 1998. NIST-JANAF thermochemical tables - fourth edition. Part I, Al-Co. J. Phys. Chem. Ref. Data Monograph 9, 1951.

Ciavatta, L., 1980. The specific interaction theory in evaluating ionic equilibria. Ann. Chim. Roma 70, 551–567.

Courdouan Merz, A., 2008. Nature and Reactivity of Dissolved Organic Matter in Clay Formations Evaluated for the Storage of Radioactive Waste. ETH Zürich, Zürich, Switzerland, p. 114. https://doi.org/10.3929/ethz-a-005680592. PhD Thesis.

Cox, J.D., Wagman, D.D., Medvedev, V.A., 1989. CODATA Key Values for Thermodynamics. Hemisphere Publishing Corp., New York, USA.

Crançon, P., Mangeret, A., De Windt, L., 2012. Assessing migration of uranium through chalk substrate: field study and reactive transport modelling. Int. J. Environ. Pollut Remed. 1, 59–66. https://doi.org/10.11159/ijepr.2012.009.

Cross, J.E., Ewart, F.T., 1991. Hatches — a thermodynamic database and management system. Radiochim. Acta 52–53, 421–422. https://doi.org/10.1524/ract.1991.5253.2.421.

Curti, E., Fujiwara, K., Iijima, K., Tits, J., Cuesta, C., Kitamura, A., Glaus, M.A., Muller, W., 2010. Radium uptake during barite recrystallization at 23 ± 2 °C as a function of solution composition: an experimental ^{133}Ba and ^{226}Ra tracer study. Geochem. Cosmochim. Acta 74, 3553–3570. https://doi.org/10.1016/j.gca.2010.03.018.

Davies, C.W., 1962. Ion Association. Butterworths, London, UK.

De Craen, M., Wang, L., Van Geet, M., Moors, H., 2004. Geochemistry of Boom Clay Pore Water at the Mol Site. SCK•CEN. SCK•CEN-BLG-990, p. 181. http://inis.iaea.org/search/search.aspx?orig_q=RN:36097549.

Dong, W., Brooks, S.C., 2006. Determination of the formation constants of ternary complexes of uranyl and carbonate with alkaline earth metals (Mg^{2+}, Ca^{2+}, Sr^{2+}, and Ba^{2+}) using anion exchange method. Environ. Sci. Technol. 40, 4689–4695. https://doi.org/10.1021/es0606327.

Dong, W., Brooks, S.C., 2008. Formation of aqueous $MgUO_2(CO_3)_3^{2-}$ complex and uranium anion exchange mechanism onto an exchange resin. Environ. Sci. Technol. 42, 1979–1983. https://doi.org/10.1021/es0711563.

Doughman, M.S., O'Shea, K.E., Qafoku, N.P., Emerson, H.P., Szecsody, J.E., Carroll, K.C., Katsenovich, Y.P., 2024. Impact of chromium (VI) as a co-contaminant on the sorption and co-precipitation of uranium (VI) in sediments under mildly alkaline oxic conditions. J. Environ. Manag. 349, 119463 https://doi.org/10.1016/j.jenvman.2023.119463.

Dumas, T., Guigue, M., Moisy, P., Colina-Ruiz, R., de Leon, J.M., Matara-Aho, M., Solari, P.L., Monfort, M., Moulin, C., Beccia, M.R., Den Auwer, C., 2018. Experimental speciation of plutonium(IV) in natural seawater. ChemistrySelect 3, 2021–2024. https://doi.org/10.1002/slct.201702762.

Emrén, A.T., Arthur, R., Glynn, P.D., McMurry, J., 1999. The modeler's influence on calculated solubilities for performance assessments at the Äspö Hard-Rock Laboratory. Mater. Res. Soc. Symp. Proc. 556, 559–566. https://doi.org/10.1557/PROC-556-559.

Endrizzi, F., Leggett, C.J., Rao, L., 2016. Scientific basis for efficient extraction of uranium from seawater. I: understanding the chemical speciation of uranium under seawater conditions. Ind. Eng. Chem. Res. 55, 4249–4256. https://doi.org/10.1021/acs.iecr.5b03679.

Endrizzi, F., Rao, L., 2014. Chemical speciation of uranium(VI) in marine environments: complexation of calcium and magnesium ions with $[(UO_2)(CO_3)_3^{4-}]$ and the effect on the extraction of uranium from seawater. Chem. Eur J. 20, 14499–14506. https://doi.org/10.1002/chem.201403262.

Gardner, C.B., Wichterich, C., Calero, A.E., Welch, S.A., Widom, E., Smith, D.F., Carey, A. E., Lyons, W.B., 2022. Carbonate weathering, phosphate fertilizer, and hydrologic controls on dissolved uranium in rivers in the US Corn Belt: disentangling seasonal geogenic- and fertilizer-derived sources. Sci. Total Environ. 861, 160455 https://doi.org/10.1016/j.scitotenv.2022.160455.

Gaucher, E.C., Tournassat, C., Pearson, F.J., Blanc, P., Crouzet, C., Lerouge, C., Altmann, S., 2009. A robust model for pore-water chemistry of clayrock. Geochem. Cosmochim. Acta 73, 6470–6487. https://doi.org/10.1016/j.gca.2009.07.02.

Geipel, G., Amayri, S., Bernhard, G., 2008. Mixed complexes of alkaline earth uranyl carbonates: a laser-induced time-resolved fluorescence spectroscopic study. Spectrochim. Acta, Part A 71, 53–58. https://doi.org/10.1016/j.saa.2007.11.007.

Giffaut, E., Grivé, M., Blanc, P., Vieillard, P., Colàs, E., Gailhanou, H., Gaboreau, S., Marty, N., Madé, B., Duro, L., 2014. Andra thermodynamic database for performance assessment: ThermoChimie. Appl. Geochem. 49, 225–236. https://doi.org/10.1016/j.apgeochem.2014.05.007.

Grenthe, I., Fuger, L., Konings, R.G.M., Lemire, R.J., Muller, A.B., Nguyen-Trung, C., Wanner, H., 1992. Chemical Thermodynamics 1. Chemical Thermodynamics of Uranium. North Holland Elsevier Science Publishers B. V., Amsterdam, The Netherlands. http://www.oecd-nea.org/dbtdb/pubs/uranium.pdf.

Grenthe, I., Gaona, X., Plyasunov, A.V., Rao, L., Runde, W.H., Grambow, B., Koning, R.J. M., Smith, A.L., Moore, E.E., 2020. Chemical Thermodynamics 14. Second Update on the Chemical Thermodynamics of Uranium, Neptunium, Plutonium, Americium and Technetium. OECD Nuclear Energy Agency Data Bank. OECD Publications, Paris, France. http://www.oecd-nea.org/jcms/pl_46643/second-update-of-u-np-pu-am-and-tc.

Grenthe, I., Hummel, W., Puigdomènech, I., 1997. Chapter III. Chemical background for the modelling of reactions in aqueous systems. In: Grenthe, I., Puigdomènech, I. (Eds.), Modelling in Aquatic Chemistry. OECD, Paris, pp. 69–130. http://www.oecd-nea.org/dbtdb/pubs/book-pdf/069-130.pdf.

Grenthe, I., Monpean, F., Spahiu, K., Wanner, H., 2013. TDB-2. Guidelines for the Extrapolation to Zero Ionic Strength. OECD Nuclear Energy Agency, Data Bank, p. 78. http://www.oecd-nea.org/jcms/pl_37492/tdb-2-guidelines-for-the-extrapolation-to-zero-ionic-strength.

Grivé, M., Duro, L., Colàs, E., Giffaut, E., 2015. Thermodynamic data selection applied to radionuclides and chemotoxic elements: an overview of the ThermoChimie-TDB. Appl. Geochem. 55, 85–94. https://doi.org/10.1016/j.apgeochem.2014.12.017.

Guillaumont, R., Fanghänel, T., Fuger, J., Grenthe, I., Neck, V., Palmer, D.A., Rand, M., 2003. Chemical Thermodynamics 5. Update on the Chemical Thermodynamics of Uranium, Neptunium, Plutonium, Americium and Technetium. North Holland Elsevier Science Publishers B. V., Amsterdam, The Netherlands. http://www.oecd-nea.org/dbtdb/pubs/vol5-update-combo.pdf. http://www.oecd-nea.org/dbtdb/pubs/Errata_Update.pdf.

Honty, M., Frederickx, L., Wang, L., De Craen, M., Thomas, P., Moors, H., Jacops, E., 2022. Boom Clay pore water geochemistry at the Mol site: experimental data as determined by in situ sampling of the piezometers. Appl. Geochem. 136, 105156 https://doi.org/10.1016/j.apgeochem.2021.105156.

Hummel, W., Anderegg, G., Rao, L.F., Puigdomènech, I., Tochiyama, O., 2005. Chemical Thermodynamics 9. Chemical Thermodynamics of Compounds and Complexes of U, Np, Pu, Am, Tc, Se, Ni and Zr with Selected Organic Ligands. North Holland Elsevier Science Publishers B. V., Amsterdam, The Netherlands. http://www.oecd-nea.org/dbtdb/pubs/vol9-organic-ligands.pdf.

Hummel, W., Filella, M., Rowland, D., 2019. Where to find equilibrium constants? Sci. Total Environ. 692, 49–59. https://doi.org/10.1016/j.scitotenv.2019.07.161.

Irving, H., Rossotti, H., 1956. Some relationships among the stabilities of metal complexes. Acta Chem. Scand. 10, 72–93. https://doi.org/10.3891/acta.chem.scand.10-0072.

Jo, Y., Cho, H.-R., Yun, J.-I., 2020. Visible-NIR absorption spectroscopy study of the formation of ternary plutonyl(VI) carbonate complexes. Dalton Trans. 49, 11605–11612. https://doi.org/10.1039/d0dt01982h.

Jo, Y., Kim, H.-K., Yun, J.-I., 2019a. Complexation of $UO_2(CO_3)_3^{4-}$ with Mg^{2+} at varying temperatures and its effect on U(VI) speciation in groundwater and seawater. Dalton Trans. 48, 14769–14776. https://doi.org/10.1039/c9dt03313k.

Jo, Y., Kirishima, A., Kimuro, S., Kim, H.-K., Yun, J.-I., 2019b. Formation of $CaUO_2(CO_3)_3^{2-}$ and $Ca_2UO_2(CO_3)_3$(aq) complexes at variable temperatures (10 – 70 °C). Dalton Trans. 48, 6942–6950. https://doi.org/10.1039/c9dt01174a.

Jo, Y., Lee, J.-Y., Yun, J.-I., 2022. Chemical thermodynamics of ternary M-An(VI)-CO_3 system (M = Mg, Ca, Sr, and Ba). Radiochim. Acta 110, 873–889. https://doi.org/10.1515/ract-2021-1133.

Kalmykov, S.N., Choppin, G.R., 2000. Mixed $Ca^{2+}/UO_2^{2+}/CO_3^{2-}$ complex formation at different ionic strengths. Radiochim. Acta 88, 603–606. https://doi.org/10.1524/ract.2000.88.9-11.603.

Kelly, S.D., Kemner, K.M., Brooks, S.C., 2007. X-ray absorption spectroscopy identifies calcium-uranyl-carbonate complexes at environmental concentrations. Geochem. Cosmochim. Acta 71, 821–834. https://doi.org/10.1016/j.gca.2006.10.013.

Kelly, S.D., Kemner, K.M., Brooks, S.C., Fredrickson, J.K., Carroll, S.L., Kennedy, D.W., Zachara, J.M., Plymale, A.E., Fendorf, S., 2005. Ca-UO_2-CO_3 complexation - implications for bioremediation of U(VI). Phys. Scripta T115, 915–917. https://doi.org/10.1238/Physica.Topical.115a00915.

Kerisit, S., Liu, C., 2010. Molecular simulation of the diffusion of uranyl carbonate species in aqueous solution. Geochem. Cosmochim. Acta 74, 4937–4952. https://doi.org/10.1016/j.gca.2010.06.007.

Kinniburgh, D.G., Cooper, D.M., 2011. Creating Graphical Output with PHREEQC. http://www.phreeplot.org.

Kossiakoff, A., Harker, D., 1938. The calculation of the ionization constants of inorganic oxygen acids from their structures. J. Am. Chem. Soc. 60, 2047–2055. https://doi.org/10.1021/ja01276a010.

Lartigue, J.E., Charrasse, B., Reile, B., Descostes, M., 2020. Aqueous inorganic uranium speciation in European stream waters from the FOREGS dataset using geochemical modelling and determination of U bioavailability baseline. Chemosphere 251, 126302. https://doi.org/10.1016/j.chemosphere.2020.126302.

Lee, J.-Y., Vespa, M., Gaona, X., Dardenne, K., Rothe, J., Rabung, T., Altmaier, M., Yun, J.-I., 2017. Formation, stability and structural characterization of ternary $MgUO_2(CO_3)_3^{2-}$ and $Mg_2UO_2(CO_3)_3$(aq) complexes. Radiochim. Acta 105, 171–185. https://doi.org/10.1515/ract-2016-2643.

Lee, J.-Y., Yun, J.-I., 2013. Formation of ternary $CaUO_2(CO_3)_3^{2-}$ and $Ca_2UO_2(CO_3)_3$(aq) complexes under neutral to weakly alkaline conditions. Dalton Trans. 42, 9862–9869. https://doi.org/10.1039/c3dt50863c.

Lee, J.Y., Amayri, S., Montoya, V., Fellhauer, D., Gaona, X., Altmaier, M., 2019. Solubility and stability of liebigite, $Ca_2UO_2(CO_3)_3{\cdot}10H_2O$(cr), in dilute to concentrated NaCl and $NaClO_4$ solutions at T = 22-80 °C. Appl. Geochem. 111, 104374 https://doi.org/10.1016/j.apgeochem.2019.104374.

Lemire, R.J., Berner, U., Musikas, C., Palmer, D.A., Taylor, P., Tochiyama, O., 2013. Chemical Thermodynamics 13a. Chemical Thermodynamics of Iron. Part 1. OECD Nuclear Energy Agency Data Bank. OECD Publications, Paris, France. http://www.oecd-nea.org/dbtdb/pubs/6355-vol13a-iron.pdf.

Lemire, R.J., Fuger, J., Nitsche, H., Potter, P., Rand, M., Rydberg, J., Spahiu, K., Sullivan, J.C., Ullman, W.J., Vitorge, P., Wanner, H., 2001. Chemical Thermodynamics 4. Chemical Thermodynamics of Neptunium and Plutonium. North Holland Elsevier Science Publishers B. V., Amsterdam, The Netherlands. http://www.oecd-nea.org/dbtdb/pubs/vol4-neptunium-plutonium.pdf.

Lemire, R.J., Palmer, D.A., Taylor, P., Schlenz, H., 2020. Chemical thermodynamics 13b. Chemical Thermodynamics of Iron. Part 2. OECD Nuclear Energy Agency Data Bank. OECD Publications, Paris, France. http://www.oecd-nea.org/dbtdb/pubs/7499-vol13b-iron.pdf.

Lestini, L., Beaucaire, C., Vercouter, T., Ballini, M., Descostes, M., 2019. Role of trace elements in the 226-radium incorporation in sulfate minerals (gypsum and celestite). ACS Earth Space Chem. 3, 295–304. https://doi.org/10.1021/acsearthspacechem.8b00150.

Liu, C.X., Jeon, B.H., Zachara, J.M., Wang, Z.M., 2007. Influence of calcium on microbial reduction of solid phase uranium(VI). Biotechnol. Bioeng. 97, 1415–1422. https://doi.org/10.1002/bit.21357.

Maia, F.M.S., Ribet, S., Bailly, C., Grivé, M., Madé, B., Montavon, G., 2021. Evaluation of thermodynamic data for aqueous Ca-U(VI)-CO_3 species under conditions characteristic of geological clay formation. Appl. Geochem. 124, 104844 https://doi.org/10.1016/j.apgeochem.2020.104844.

Maloubier, M., Solari, P.L., Moisy, P., Monfort, M., Den Auwer, C., Moulin, C., 2015. XAS and TRLIF spectroscopy of uranium and neptunium in seawater. Dalton Trans. 44, 5417–5427. https://doi.org/10.1039/c4dt03547j.

McManus, J., Berelson, W.M., Klinkhammer, G.P., Hammond, D.E., Holm, C., 2005. Authigenic uranium: relationship to oxygen penetration depth and organic carbon rain. Geochem. Cosmochim. Acta 69, 95–108. https://doi.org/10.1016/j.gca.2004.06.023.

Meyer, D., Prien, R.D., Dellwig, O., Waniek, J.J., Schulz–Bull, D.E., 2014. Electrode measurements of the oxidation reduction potential in the Gotland Deep using a moored profiling instrumentation. Estuar. Coast Shelf Sci. 141, 26–36. https://doi.org/10.1016/j.ecss.2014.02.001.

Millero, F.J., Feistel, R., Wright, D.G., McDougall, T.J., 2008. The composition of Standard Seawater and the definition of the reference-composition salinity scale. Deep-Sea Res. Pt. I 55, 50–72. https://doi.org/10.1016/j.dsr.2007.10.001.

Montavon, G., Ribet, S., Hassan Loni, Y., Maia, F., Bailly, C., David, K., Lerouge, C., Madé, B., Robinet, J.C., Grambow, B., 2022. Uranium retention in a Callovo-Oxfordian clay rock formation: from laboratory-based models to *in natura* conditions. Chemosphere 299, 134307. https://doi.org/10.1016/j.chemosphere.2022.134307.

Montoya, V., Noseck, U., Mattick, F., Britz, S., Blechschmidt, I., Schäfer, T., 2021. Radionuclide geochemistry evolution in the long-term in-situ test (LIT) at grimsel test site (Switzerland). J. Hazard Mater. 424, 127733 https://doi.org/10.1016/j.jhazmat.2021.127733.

Murphy, W.M., Shock, E.L., 1999. Environmental aqueous geochemistry of actinides. In: Burns, P.C., Finch, R. (Eds.), Uranium: Mineralogy, Geochemistry and the Environment, vol. 38. Mineralogical Society of America, Washington, DC, USA, pp. 221–253.

Naumov, G.B., Ryzhenko, B.N., Khodakovsky, I.L., 1974. Handbook of Thermodynamic Data. U.S. Geological Survey. USGS-WRD-74-001, p. 328.

Neck, V., Altmaier, M., Seibert, A., Yun, J.I., Marquardt, C.M., Fanghänel, T., 2007. Solubility and redox reactions of Pu(IV) hydrous oxide: evidence for the formation of PuO_{2+x}(s, hyd). Radiochim. Acta 95, 193–207. https://doi.org/10.1524/ract.2007.95.4.193.

Nelson, D.M., Lovett, M.B., 1978. Oxidation state of plutonium in Irish Sea. Nature 276, 599–601. https://doi.org/10.1038/276599a0.

Neuilly, M., 1998. Modélisation et estimation des erreurs de mesures, Edition. Lavoisier, Technique & Documentation, Paris.

Nordstrom, D.K., Plummer, L.N., Wigley, T.M.L., Wolery, T.J., Ball, J.W., Jenne, E.A., Bassett, R.L., Crerar, D.A., Florence, T.M., Fritz, B., Hoffman, M., Holdren Jr., G.R., Lafon, G.M., Mattigod, S.V., McDuff, R.E., Morel, F., Reddy, M.M., Sposito, G., Thrailkill, J., 1979. A comparison of computerized chemical models for equilibrium calculations in aqueous systems. In: Jenne, E.A. (Ed.), Chemical Modeling in Aqueous Systems. American Chemical Society, Washington, DC, USA, pp. 857–892.

Oher, H., Vercouter, T., Réal, F., Shang, C., Reiller, P.E., Vallet, V., 2020. Influence of alkaline earth metal ions on structures and luminescent properties of $Na_mM_nUO_2(CO_3)_3^{(4-m-2n)-}$ (M = Mg, Ca; m, n = 0–2): time-resolved fluorescence spectroscopy and *ab initio* studies. Inorg. Chem. 59, 15036–15049. https://doi.org/10.1021/acs.inorgchem.0c01986.

Parkhurst, D.L., Appelo, C.A.J., 1999. User's guide to PHREEQC (version 2) — a computer program for speciation. Batch-Reaction, One-Dimensional Transport, and Inverse Geochemical Calculations. U.S. Geological Survey 99–4259. http://wwwbrr.cr.usgs.gov/projects/GWC_coupled/phreeqci/.

Parkhurst, D.L., Appelo, C.A.J., 2013. Description of Input and Examples for PHREEQC Version 3 — A Computer Program for Speciation, Batch-Reaction, One-Dimensional Transport, and Inverse Geochemical Calculations. U.S. Geological Survey., p. 497 (Chapter 43) of Section A, Groundwater Book 6, Modeling Techniques. http://pubs.usgs.gov/tm/06/a43/pdf/tm6-A43.pdf

Plummer, L.N., Busenberg, E., 1982. The solubilities of calcite, aragonite and vaterite in CO_2-H_2O solutions between 0 and 90°C, and an evaluation of the aqueous model for the system $CaCO_3$-CO_2-H_2O. Geochem. Cosmochim. Acta 46, 1011–1040. https://doi.org/10.1016/0016-7037(82)90056-4.

Plyasunova, N.V., Zhang, Y., Muhammed, M., 1998. Critical evaluation of thermodynamics of complex formation of metal ions in aqueous solutions. V. Hydrolysis and hydroxo-complexes of Co^{2+} at 298.15 K. Hydrometallurgy 48, 153–169. https://doi.org/10.1016/S0304-386X(97)00078-9.

Powell, K.J., Brown, P.L., Byrne, R.H., Gajda, T., Hefter, G., Leuz, A.-K., Sjöberg, S., Wanner, H., 2009. Chemical speciation of environmentally significant metals with inorganic ligands. Part 3: the Pb^{2+} + OH^-, Cl^-, CO_3^{2-}, SO_4^{2-}, and PO_4^{3-} systems (IUPAC Technical Report). Pure Appl. Chem. 81, 2425–2476. https://doi.org/10.1351/pac-rep-09-03-05.

Powell, K.J., Brown, P.L., Byrne, R.H., Gajda, T., Hefter, G., Leuz, A.-K., Sjöberg, S., Wanner, H., 2011. Chemical speciation of environmentally significant metals with inorganic ligands. Part 4: the Cd^{2+} + OH^-, Cl^-, CO_3^{2-}, SO_4^{2-}, and PO_4^{3-} systems (IUPAC Technical Report). Pure Appl. Chem. 83, 1163–1214. https://doi.org/10.1351/pac-rep-10-08-09.

Powell, K.J., Brown, P.L., Byrne, R.H., Gajda, T., Hefter, G., Sjoberg, S., Wanner, H., 2007. Chemical speciation of environmentally significant metals with inorganic ligands - Part 2: the Cu^{2+}–OH^-, Cl-, CO_3^{2-}, SO_4^{2-}, and PO_4^{3-} systems - (IUPAC technical report). Pure Appl. Chem. 79, 895–950. https://doi.org/10.1351/pac200779050895.

Prat, O., Vercouter, T., Ansoborlo, E., Fichet, P., Perret, P., Kurttio, P., Salonen, L., 2009. Uranium speciation in drinking water from drilled wells in southern Finland and its potential links to health effects. Environ. Sci. Technol. 43, 3941–3946. https://doi.org/10.1021/es803658e.

Priest, C., Tian, Z.Q., Jiang, D.E., 2016. First-principles molecular dynamics simulation of the $Ca_2UO_2(CO_3)_3$ complex in water. Dalton Trans. 45, 9812–9819. https://doi.org/10.1039/c5dt04576b.

Rai, D., Hess, N.J., Felmy, A.R., Moore, D.A., Yui, M., 1999a. A thermodynamic model for the solubility of NpO_2(am) in the aqueous K^+-HCO_3^--CO_3^{2-}-OH^--H_2O system. Radiochim. Acta 84, 159–169. https://doi.org/10.1524/ract.1999.84.3.159.

Rai, D., Hess, N.J., Felmy, A.R., Moore, D.A., Yui, M., Vitorge, P., 1999b. A thermodynamic model for the solubility of PuO_2(am) in the aqueous K^+-HCO_3^--CO_3^{2-}-OH^--H_2O system. Radiochim. Acta 86, 89–99. https://doi.org/10.1524/ract.1999.86.34.89.

Reiller, P., 2022. The PRODATA Thermochemical Database – A Database Applied for Uranium Mining Operations. Commissariat à l'Énergie Atomique et aux Énergies Alternatives. CEA-R 6573 (ISSN 0429-3460) p. 228. http://hal-cea.archives-ouvertes.fr/cea-03757400.

Reiller, P.E., Descostes, M., 2020. Development and application of the thermodynamic database PRODATA dedicated to the monitoring of mining activities from exploration to remediation. Chemosphere 251, 126301. https://doi.org/10.1016/j.chemosphere.2020.126301.

Reiller, P.E., Marang, L., Jouvin, D., Benedetti, M.F., 2012. Uranium (VI) binding to humic substances: speciation, estimation of competition, and application to independent data. In: Merkel, B., Schipek, M. (Eds.), The New Uranium Mining Boom. Challenge and Lessons Learned. Springer-Verlag, Berlin, Germany, pp. 565–572. https://doi.org/10.1007/978-3-642-22122-4_65.

Robie, R.A., Hemingway, B.S., 1995. Thermodynamic properties of minerals and related substances at 298.15 K and 1 bar (10^5 pascal) pressure and at higher temperatures. US Geological Survey 2131, 461. http://pubs.usgs.gov/bul/2131/report.pdf.

Shang, C., Coreau, N., Macé, N., Descostes, M., Reiller, P.E., 2023. Implications of recently derived thermodynamic data for $(Mg/Ca)_nUO_2(CO_3)_3^{(4-2n)-}$ complexes on the predominance of the Mg^{2+}–Ca^{2+}–UO_2^{2+}–OH^-–CO_3^{2-} systems, and application to natural and legacy-mining waters. Sci. Total Environ. 858, 159927 https://doi.org/10.1016/j.scitotenv.2022.159927.

Shang, C., Reiller, P.E., 2020. Determination of formation constants and specific ion interaction coefficients for $Ca_nUO_2(CO_3)_3^{(4-2n)-}$ complexes in NaCl solution by time-resolved laser-induced luminescence spectroscopy. Dalton Trans. 49, 466–481. https://doi.org/10.1039/c9dt03543e.

Shang, C., Reiller, P.E., 2021a. The determination of the thermodynamic constant of $MgUO_2(CO_3)_3^{2-}$ complex in $NaClO_4$ and NaCl media using time-resolved luminescence spectroscopy, and applications to different geochemical contexts. Dalton Trans. 50, 4363–4379. https://doi.org/10.1039/d0dt04124f.

Shang, C., Reiller, P.E., 2021b. Effect of temperature on the complexation of triscarbonatouranyl(VI) with calcium and magnesium in NaCl aqueous solution. Dalton Trans. 50, 17165–17180. https://doi.org/10.1039/d1dt03204f.

Shang, C., Reiller, P.E., Vercouter, T., 2020. Spectroluminescence measurements of stability constants of $Ca_nUO_2(CO_3)_3^{(4-2n)-}$ complexes in $NaClO_4$ medium and investigation of interaction effects. Dalton Trans. 49, 15443–15460. https://doi.org/10.1039/d0dt03164j.

Shannon, R.D., 1976. Revised effective ionic radii and systematic studies of interatomic distances in halides and chalcogenides. Acta Crystallogr., Sect. A 32, 751–767. https://doi.org/10.1107/S0567739476001551.

Shock, E.L., Koretsky, C.M., 1995. Metal-organic complexes in geochemical processes: estimation of standard partial molal thermodynamic properties of aqueous complexes between metal-cations and monovalent organic acid ligands at high pressures and temperatures. Geochem. Cosmochim. Acta 59, 1497–1532. https://doi.org/10.1016/0016-7037(95)00058-8.

Sillén, L.G., Martell, A.E., 1964. Stability Constants of Metal Ion Complexes. Chemical Society, London, U.K.

Silva, R.J., Bidoglio, G., Rand, M., Robouch, P., Wanner, H., Puigdomènech, I., 1995. In: Sandino, M.C.A., Puigdomènech, I., Rand, M.H. (Eds.), Chemical Thermodynamics 2. Chemical Thermodynamics of Americium with an Appendix on Chemical Thermodynamics of Uranium (Grenthe, I.. North Holland Elsevier Science Publishers B. V., Amsterdam, The Netherlands. http://www.oecd-nea.org/dbtdb/pubs/americium.pdf.

Smolíková, V., Pelcová, P., Ridošková, A., Leermakers, M., 2022. Diffusive Gradients in Thin-films technique for uranium monitoring along a salinity gradient: a comparative study on the performance of Chelex-100, Dow-PIWBA, Diphonix, and Lewatit FO 36 resin gels in the Scheldt estuary. Talanta 240, 123168. https://doi.org/10.1016/j.talanta.2021.123168.

Sverjensky, D.A., Shock, E.L., Helgeson, H.C., 1997. Prediction of the thermodynamic properties of aqueous metal complexes to 1000°C and 5 kb. Geochem. Cosmochim. Acta 61, 1359–1412. https://doi.org/10.1016/s0016-7037(97)00009-4.

Thury, M., Bossart, P., 1999. Mont-Terri Rock Laboratory. Results of the hydrogeological, geochemical and geotechnical experiments performed in 1996 and 1997. Swiss National Hydrological and Geological Survey. Rapport Géologique Nr 23, 234. http://www.mont-terri.ch/content/mont-terri-internet/en/documentation/publications-from-swisstopo.download/mont-terri-internet/en/publications/publications-swisstopo/GBD-23.pdf.

Tirler, A.O., Hofer, T.S., 2016. The structural influence of Ca^{2+} counter-ions on uranyl (VI) tricarbonate in aqueous solution. Dalton Trans. 45, 4983–4988. https://doi.org/10.1039/c5dt04718h.

Tullborg, E.L., Suksi, J., Geipel, G., Krall, L., Auque, L., Gimeno, M., Puigdomènech, I., 2017. The occurrences of $Ca_2UO_2(CO_3)_3$ complex in Fe(II) containing deep groundwater at Forsmark, eastern Sweden. Proced. Earth Plan. Sci. 17, 440–443. https://doi.org/10.1016/j.proeps.2016.12.111.

Vercouter, T., 2021. Chimie des actinides. Complexes et solides en milieux aqueux. Techniques de l'Ingénieur. BN3520 V2, p. 18. http://www.techniques-ingenieur.fr/res/pdf/encyclopedia/42457210-bn3520.pdf.

Vinsot, A., Mettler, S., Wechner, S., 2008. In situ characterization of the Callovo-Oxfordian pore water composition. Phys. Chem. Earth 33, S75–S86. https://doi.org/10.1016/j.pce.2008.10.048.

Vitorge, P., 1999. Chimie des actinides. Techniques de l'Ingénieur. BN 3520 v1, p. 13. http://www.techniques-ingenieur.fr/res/pdf/encyclopedia/tiabn-bn3520-version1.pdf.

Vitorge, P., Capdevila, H., 2003. Thermodynamic data for modelling actinide speciation in environmental waters. Radiochim. Acta 91, 623. https://doi.org/10.1524/ract.91.11.623.23466, 361.

Wagman, D.D., Evans, W.H., Parker, V.B., Schumm, R.H., Halow, I., Bailey, S.M., Churney, K.L., Nuttall, R.L., 1982. The NBS Tables of chemical thermodynamic properties. Selected values for inorganic and C_1 and C_2 organic substances in SI units. J. Chem. Ref. Data 11, 392.

Wang, L., Honty, M., De Craen, M., Frederickx, L., 2023. Boom Clay pore-water geochemistry at the Mol site: chemical equilibrium constraints on the concentrations of major elements. Appl. Geochem. 148, 105541 https://doi.org/10.1016/j.apgeochem.2022.105541.

Xie, J.C., Wang, J.L., Lin, J.F., 2021. New insights into the role of calcium in the bioreduction of uranium(VI) under varying pH conditions. J. Hazard Mater. 411, 125140 https://doi.org/10.1016/j.jhazmat.2021.125140.

Yamaguchi, T., Sakamoto, Y., Ohnuki, T., 1994. Effect of the complexation on solubility of Pu(IV) in aqueous carbonate system. Radiochim. Acta 66–67, 9–14. https://doi.org/10.1524/ract.1994.6667.s1.9.

Zhang, Y., Muhammed, M., 2001. Critical evaluation of thermodynamics of complex formation of metal ions in aqueous solutions: VI. Hydrolysis and hydroxo-complexes of Zn^{2+} at 298.15 K. Hydrometallurgy 60, 215–236. https://doi.org/10.1016/S0304-386X(01)00148-7.